CHAPTER **10**

# GaAs-Based Quantum Dot Lasers

**Mark T. Crowley,*** **Nader A. Naderi,[†]** **Hui Su,[‡]**
**Frederic Grillot,[§,‖]** and **Luke F. Lester***

\* Center for High Technology Materials, University of New Mexico, USA
† US Air Force Research Laboratory, Kirtland Air Force Base, USA
‡ Fujian Institute of Research on the Structure of Matter, Fuzhou, Fujian, Fuzhou, P.R. China
§ Université Européenne de Bretagne, Institut National des Sciences Appliquées, CNRS FOTON, France
‖ Telecom Paristech, Ecole Nationale Supérieure des Télécommunications, CNRS LTCI, Paris, France

# 1. INTRODUCTION

The three-dimensional confinement of electrons and holes in a semiconductor quantum dot (QD) profoundly changes its density of states compared to a bulk semiconductor or thin-film quantum well (QW). In practical ensembles of QDs, the ideal delta-function density of states of a single dot is modified into a nearly Gaussian contour that is determined by the degree of inhomogeneity in the QD sizes and shapes. For InAs QD laser diodes grown on a GaAs substrate, however, this so-called inhomogeneous broadening of the QD distribution frequently does not deter these devices from demonstrating unique and state-of-the-art operating characteristics. In fact without some QD nonuniformity, a QD distributed feedback (DFB) laser would not be possible over a significant temperature range due to the mismatched wavelength shifts of the refractive index and optical gain that are present in any semiconductor. Thus, in this chapter, some of the unique advantages of GaAs-based QD lasers at wavelengths longer than 1.2μm will be reviewed. In Sections 2.1-2.4, the ultralow-threshold current density and remarkable improvements in temperature stability that have been accomplished with the InAs/InGaAs QD Fabry–Perot (FP) lasers on GaAs will be discussed. In Section 3, the intriguing efforts to measure, model, and manipulate the extreme behavior of the linewidth enhancement factor in QD lasers will be described and compared to that of QW lasers. In Section 4, the special features of QD DFB lasers will be discussed, including the ultralow linewidth–power product and the exceptional optical feedback insensitivity that have been observed. Finally, for the segment of QD laser research that could benefit from improved dot uniformity, the progress in understanding the limitations of achieving higher modulation bandwidths in directly modulated and injection-locked QD lasers will be detailed (Section 5).

# 2. ULTRALOW-THRESHOLD AND TEMPERATURE-INSENSITIVE OPERATION

In this section, a review of the temperature performance of InGaAs/GaAs QD laser materials emitting at wavelengths longer than 1.2μm is presented. The concept of introducing an atomic-like density of states surrounded by conventional semiconductor material was predicted to result in a

revolutionary laser material, especially in terms of the temperature-insensitive operation (Arakawa and Sakaki, 1982). Almost three decades of intense research has led to technological advances that have now positioned the QD laser not only as an ultralow-threshold semiconductor laser (SL) (Deppe et al., 2009; Eliseev et al., 2000; Sellers et al., 2004; Salhi et al., 2008; Shimizu et al., 2005), the best being in the vicinity of $10 A/cm^2$ per dot layer, but also as a candidate for uncooled high-temperature applications ranging from optical interconnects within multi-core architectures to sensing applications essential to oil and gas exploration. Uncooled QD lasers provide a cost-effective technology solution due to the reduction of device packaging complexity and the elimination of power-hungry cooling requirements that are typically associated with SLs. The highest reported uncooled operating temperatures for InGaAs/GaAs QD lasers have been quite impressive, demonstrating lasing operation beyond $195\,°C$ from the QD ground-state transition (QD Laser Inc., 2011; Tokranov et al., 2003).

## 2.1. Ultralow-threshold current densities

Historically, one of the key reasons for the development of semiconductor quantum dot lasers was the prediction of ultralow-threshold current densities (Arakawa and Sakaki, 1982). Indeed, since the introduction of the QD lasers, several research groups have reported ultralow-threshold current densities, surpassing the best QW results $\sim50 A/cm^2$ (Chand et al., 1991) by almost an order of magnitude. In particular, the inception of the "dots-in-a-well" (DWELL) design (Lester et al., 1999), which not only improves carrier capture by the dots but also increases the density of QDs and hence the material gain, has allowed for record threshold values to be realized. According to the DWELL strain-reducing design, rather than growing on and capping the InAs dots with GaAs, the dots are grown on a thin layer of InGaAs and subsequently capped by the same material with typical indium compositions of 15%. At the turn of the millennium, a threshold current density of $26 A/cm^2$ was achieved based on this technological advancement for a single DWELL layer (Liu et al., 1999). A further reduction in threshold current density to $16 A/cm^2$ was enabled by applying high-reflectivity dielectric coatings to both facets (Eliseev et al., 2000). Most recently, an extremely low CW threshold current density of $8.8 A/cm^2$ for an as-cleaved 2-cm-long broad-area device with a single dot layer active region was reported (Deppe et al., 2009).

Regarding multi-stacked QD materials, an essential breakthrough was the use of high-temperature growth spacer layers (HTGSLs). Typically, the spacer layers, separating each successive dot stack consist of an initial 15nm of GaAs grown at $510\,°C$, followed by a 35-nm HGTSL grown at $580\,°C$, with the temperature reduced back to $510\,°C$ for the growth of the next DWELL. The growth of 35nm of GaAs at this higher temperature allows the growth surface to replanarize before the growth of subsequent
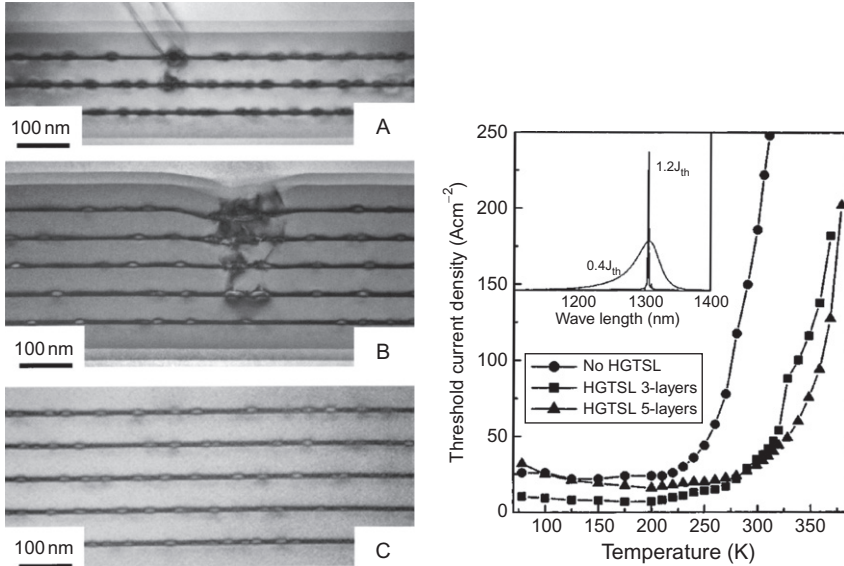
**FIGURE 10.1** *Left*: Dark field (200) TEM cross-sectional images of (A) and (B) three- and five-layer devices grown without HGTSLs and (C) a five-layer device grown with HGTSLs. The growth direction is vertically upwards for all three images. *Right*: Temperature variation of the pulsed threshold current densities for 2 three-DWELL laser devices, grown with and without HGTSLs and a five-DWELL device with HGTSLs. The cavities lengths are 5mm. The inset shows room temperature below- and above-threshold spectra for the five-DWELL HGTSL device. Adapted from Liu *et al.* (2004).

layers of dots. Incorporation of this technique during the growth of stacked dot layers has been shown to reduce surface roughness, which in turn suppresses the formation of dislocated dots. The resulting structures, shown, for example, in Fig. 10.1c, exhibit good interlayer dot uniformity (Liu *et al.*, 2004). Threshold current densities under continuous wave room-temperature operation of 32.5and 17A/cm$^2$ (10.8 and 5.6A/cm$^2$ per layer) have been reported for three-layer devices with as-cleaved facets and high-reflectivity (HR)-coated facets, respectively, comparable with the lowest reported CW values, to date, for single-layer devices (Deppe *et al.*, 2009; Eliseev *et al.*, 2000). It is well known that QD lasers still, in general, suffer from a low value of the modal gain, typically 3cm$^{-1}$ per QD layer in a multi-QD laser, due to the low areal density of the QDs and the dispersion in their size and composition. Optimization of the growth conditions, leading to superior dot uniformity in successive stacks of DWELL layers, ensures a more uniform inhomogeneous line broadening, typically <30meV. This can be maintained for as high as seven stacked DWELL layers while also keeping a relatively high dot density in each individual layer (Salhi *et al.*, 2008). This effort, for example, has led Salhi *et al.* to obtain a low threshold of 10A/cm$^2$ for a multi-stack

DWELL structure with 0.6-mm long cavity and high-reflectivity coatings on both facets (Salhi *et al.*, 2008). The dots are extremely sensitive to the level of strain they experience; therefore, one would like to recover the same surface and hence nominal strain conditions for each QD layer. For a 12-layer device with high-reflectivity coatings, a record low value of 7 A/cm$^2$ per layer was achieved (Shimizu *et al.*, 2005). In particular, high-reflectivity coatings promote low-threshold current densities by reducing the threshold gain requirements through a reduction in the mirror losses while concomitantly reducing the carrier lifetime, thereby additionally minimizing current parasitics. Short-cavity devices incorporating high-reflectivity facet coatings will be discussed in Section 2.4.

## 2.2. Undoped QD lasers: Temperature performance

The proposal that the threshold current density of QD lasers would be relatively temperature insensitive (Arakawa and Sakaki, 1982) marked an era of research dedicated to the demonstration of the ultimate temperature-immune SL. Such temperature insensitivity was predicted as a consequence of introducing full three-dimensional carrier confinement, thereby restricting charge carriers exclusively to those states involved in lasing, based on the laws of quantum mechanics. A widely used figure of merit to quantify the temperature sensitivity of the threshold current of an SL is its characteristic temperature ($T_0$), defined as:

$$T_0 = \left(\frac{\mathrm{d}\ln(J_{\mathrm{th}})}{\mathrm{d}T}\right)^{-1} \tag{10.1}$$

where $T$ is the device temperature. In general, the threshold current density, $J$th, of an SL can be decomposed into two main constituents. The first of these is associated with radiative recombination, accounting for the current at threshold consumed by this process. The other, non-radiative recombination, is viewed as a parasitic that limits the number of carriers available for radiative recombination. In an ideal laser material, each electron–hole pair entering the system should recombine radiatively and, ultimately, result in the output of a photon. In practice, this is not the case for a bulk or even QW device, with the situation deteriorating even further with increasing temperature due to the increasing thermal energy of carriers and subsequent population of higher energy states not directly involved in the lasing process.

The first laser based on InGaAs/GaAs QDs showed a superior $T_0$ value compared to competing QW materials for temperatures below 230 K (Kirstaedter *et al.*, 1994). Initially, the idea that QD lasers were advantageous for room-temperature operation and beyond was certainly questionable. However, significant progress has been made in the development of such lasers, using InAs QDs formed on a GaAs substrate

by the Stranski–Krastanow growth method (Ledentsov *et al.*, 1996; Liu *et al.*, 2000). However, these devices have remained stubbornly temperature sensitive with typical $T_0$s at room temperature of $<70\,$K (Marko *et al.*, 2005a), similar to that for InGaAsP/InP and InGaAlAs/InP QW lasers, as well as bulk material at this wavelength (Belenky *et al.*, 1999; Higashi *et al.*, 1999). A brief review is given in Marko *et al.* (2005a) of the different possible mechanisms limiting $T_0$ that have been discussed in the literature. It has been widely accepted that hot carrier effects and therefore the inevitable population of higher energy states, other than the lasing states, are the principle cause of the relatively poor $T_0$ observed in undoped QD lasers (Asryan and Suris, 1997; Crowley *et al.*, 2009; Fathpour *et al.*, 2004; Marko *et al.*, 2005a; Smowton *et al.*, 2008). Recently, a joint theoretical and experimental effort to underpin the mechanisms limiting the realization of a high $T_0$ in undoped QD lasers has revealed an interesting interplay between radiative and nonradiative recombination in 1.3-µm QD lasers (Crowley *et al.*, 2009). It was shown that although the total current density at threshold increases dramatically with increasing temperature, its radiative portion does not. There are two points to consider here. First, the higher effective mass of holes means that the hole states are more closely spaced than the electron states confined in the dots. Consequently, there are several transition energies possible from the doubly degenerate electron ground state to excited hole states before reaching the energy of the first transition involving the first electron excited states. Second, the radiative probabilities of these intermediate transitions are far smaller than that for the ground state. Thus, we have the situation that, with increasing temperature, more and more holes (and electrons) occupy excited states, which demand an ever-increasing injected carrier density to reach lasing from the ground state, but, due to the small radiative transition probabilities, this has very little effect on the radiative part of the threshold current density, which therefore appears relatively temperature insensitive. In contrast, nonradiative Auger recombination can have a similar probability for transitions involving excited states, as for those involving ground-state carriers. The sharp increase in the threshold current density at high temperatures, shown in Fig. 10.2, follows the temperature variation of the cubed threshold carrier density, confirming the key role of Auger recombination in these devices at room temperature. These results corroborate with other reports (Fathpour *et al.*, 2004) and in particular, reinforce high-pressure studies undertaken at the University of Surrey on 1.3 µm QD lasers, where Auger recombination was shown to be the dominant nonradiative recombination mechanism limiting the performance of undoped lasers above 300 K similar to QW and bulk semiconductor materials at this wavelength (Marko *et al.*, 2005a). While others have cited defect-recombination (Rossetti *et al.*, 2009) or a combination of both (Smowton *et al.*, 2008), it is clear that in a high-quality sample, Auger recombination dominates, given that it is an intrinsic process.
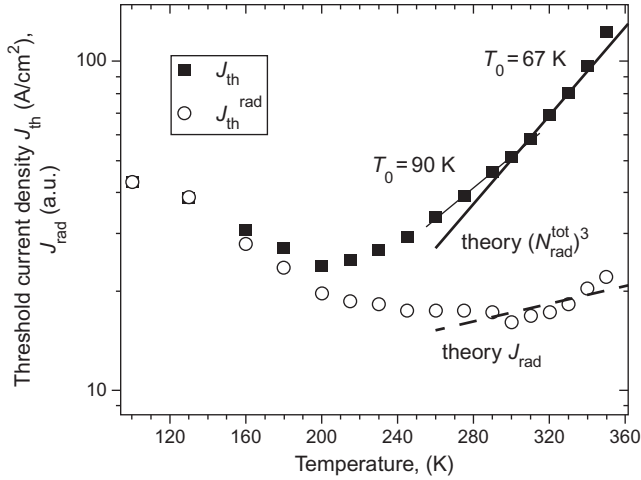
**FIGURE 10.2**   Typical temperature dependence of the threshold current density $J_{th}$ (solid symbols) and its radiative component $J_{rad}$ (open symbols) for an undoped 1.3 µm QD laser. The thick solid and dashed lines correspond to the calculated temperature variation of $(N_{th}^{tot})^3$ and $J_{rad}$, respectively. Adapted from Crowley *et al.* (2009).

There have been few exceptions to the low $T_0$ observed in typical undoped, as-cleaved QD lasers. An exemplary case of such a device was reported by Qui *et al.* in an undoped DWELL laser where a CW characteristic temperature of 86 K from 20 to 100°C was recorded. The device had four layers and produced 1.26 µm GS emission. The resultant measurements are shown in Fig. 10.3 (Qui *et al.*, 2001). More recently, for undoped devices, Salhi *et al.* reported a $T_0$ of 110 K between 10 and 85°C under CW operation for an optimized multi-stack DWELL (7 cm$^{-1}$ per layer) structure with 0.6-mm long cavity and high-reflectivity coatings on both facets (Salhi *et al.*, 2008).

## 2.3. p-Type modulation doping and advanced material concepts

In general, the best room-temperature characteristic temperatures have been made possible by p-type modulation doping. Values as high as 500 K, 700 K, and infinite as well as negative values, albeit for temperatures typically below 80°C, have been reported. The gain saturation in 1.3-µm QD lasers and therefore their $T_0$ are limited by the energy separation between the discrete levels of the dots themselves. The $T_0$ can be significantly increased by engineering the QDs to have a large energy separation between the ground and first excited radiative transitions. However, frustratingly, the hole levels are inherently much closer in energy to each other (Shchekin *et al.*, 2002), a consequence of the heavier effective mass for holes.
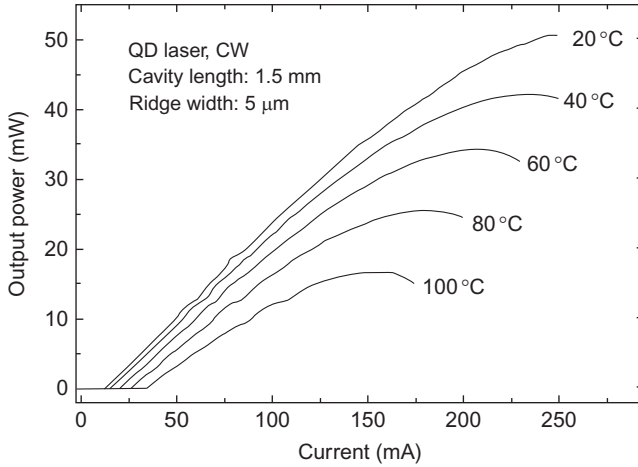
**FIGURE 10.3**   Light versus current for a 1.5-mm-cavity-length laser without facet coating measured at different temperatures. Adapted from Qiu *et al.* (2001).

In fact, the thermal spread of holes is one of the main mechanisms causing the gain to be temperature sensitive in a QD laser.

By introducing p-type modulation doping in the GaAs spacer layers between dot layers, this thermal spreading can be mitigated. The temperature dependence of the gain is then set predominantly by the electron energy levels, which are widely spaced in energy. By providing a built-in excess of holes, the effect of the closely spaced hole energy levels can be countered so that the QDs' ground-state transition is always, in principle, filled by holes. In pursuing this approach, Deppe and Shchekin achieved a $T_0$ of 161 K up to 80 °C for a doping density equivalent to 52 holes per dot in a two-stack device, and in doing so they achieved an impressive ground-state operation at temperatures as high as 167 °C. An increase of the total room-temperature ground-state gain from 9 (undoped) to 18 cm$^{-1}$ (p-doped) was observed for a laser that was otherwise the same. Considering that most undoped devices exhibit <3 cm$^{-1}$ per dot layer, the augmentation of the gain is an important ingredient in realizing high-temperature operation. As shown in Fig. 10.4, it is also interesting that from 26 to 167 °C the lasing wavelength red-shifted at a rate of 0.52 nm/°C, and the change in slope efficiency was only modest. Compared to undoped devices, the threshold of p-doped QD devices can be made temperature insensitive over a limited temperature range by compensating the small positive $T_0$ observed in undoped devices with an equal but negative $T_0$ associated with improving inter-dot transport (Marko *et al.*, 2005b). The only drawback to p-doping is that the threshold current density increases compared to an equivalent undoped device. In p-doped QD lasers, it was shown that nonradiative recombination is
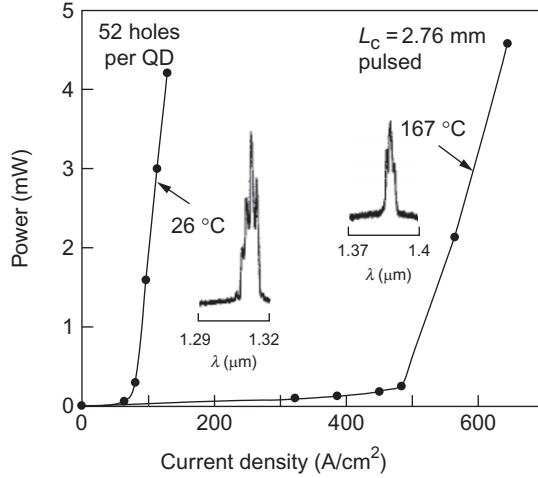
**FIGURE 10.4**    Light versus current curves and lasing spectra for the QD laser doped with 52 acceptors per QD and $L_c$=2.76 mm at room temperature and 167°C. Adapted from Shchekin and Deppe (2002).

present even at low temperature, due to the relatively large number of holes in the dots. This increases the threshold current for lasing compared to an intrinsic device, causing it to increase further with increasing temperature up to 180 K. Thermalization of electrons between the p-doped dots does not cause threshold current to decrease until above 180 K because the electrostatic attraction of the large hole population present in the dots results in an increase in the effective barrier for electron escape (Marko et al., 2005b). By introducing the correct degree of p-doping, one can cause the opposing effects of carrier thermalization and Auger recombination to cancel around room temperature, leading to an almost temperature-independent threshold current, or infinite $T_0$.

Although in p-doped structures both the gain and the $T_0$ value are ameliorated, the degree of improvement over an undoped sample is reduced at elevated temperatures. Similar to Crowley et al. (2009), Smowton et al. concluded that both Auger and defect-related nonradiative recombination limited the performance of p-doped and undoped devices due to the increasing population of higher energy dot and continuum states where nonradiative recombination increases. However, the regime of poorer $T_0$ observed in doped devices is offset to significantly higher temperatures (typically >60°C) (Smowton et al., 2008).

Tunnel injection has been used very effectively in suppressing hot carrier-related problems in QW lasers and in achieving high-speed modulation of QD lasers. Ideally in this technique, cold carriers (electrons) are injected by phonon-assisted tunneling into QD-lasing states, thereby

leading to a minimization of carrier occupation in nonlasing states. By combining p-type doping and tunnel injection, Fathpour *et al.* demonstrated an infinite $T_0$ up to 75°C for 1.3-μm QD lasers that incorporated 10 dot layers (Fathpour *et al.*, 2004). The slope efficiency also remained constant within that temperature range. The origin of the observed infinite $T_0$ was suggested to be a consequence of Auger recombination, whose rate in QDs increases upon p-doping but decreases with increasing temperature, which then offsets the increasing trend with temperature of other recombination currents that contribute to the threshold current (Fathpour *et al.*, 2004).

Researchers at the University of Albany concentrated on engineering the InAs dots for more dot uniformity by capping them with a thin layer of AlAs. This approach gave rise to more uniform dot sizes and a higher photoluminescence strength. The gain increased from 9 to $18\,\mathrm{cm}^{-1}$ compared to dots which did not include the AlAs capping layer. These lasers based on three stacks of the shape-engineered QDs showed exceptional high-temperature operation from the ground state, up to 219°C for a 7.5-mm cavity length, and 203°C for a 5.15-mm cavity length as shown in Fig. 10.5 (Tokranov *et al.*, 2003).

## 2.4. Short-cavity lasers: Temperature performance

Short-cavity HR/HR-coated devices are particularly attractive due to the extremely low $I_{\mathrm{th}}$ they exhibit, but even more so for the temperature-insensitive slope efficiencies they maintain. Zhang *et al.* presented an undoped six-stack device with QD ground-state emission at 1320nm (Zhang *et al.*, 2003). The threshold current for this device was a mere 1.5mA at room temperature for a 300-μm cavity, although the $T_0$ up to 100°C operation was just 50K. Despite this moderate $T_0$, its slope efficiency remained relatively temperature stable, demonstrating an output power of 5mW at 40mA and 100°C.

Figure 10.6 shows the CW light against current characteristics for a 0.65-mm long p-doped QD laser with HR/HR-coated mirrors. The threshold current at room temperature is 5.7mA, the maximum output power is >27mW, and the lasing wavelength is 1.29μm at 300K. The threshold current density of this five-stack device was $35\,\mathrm{A/cm}^2$ per QD layer. Figure 10.6 also shows the CW performance at temperatures of 81 and 101°C. At 81°C, the threshold current increases only slightly to 7.6mA, while the output power still exceeds 19mW. At 101°C, the threshold current increases to 9.3mA, while a maximum output power 13mW can be obtained. The inset of Fig. 10.6 shows that ground-state lasing is still achieved at a temperature as high as 161°C with lasing wavelength of 1.36μm. For a slightly longer cavity of 0.9mm, a CW $T_0$ of 213K up to 81°C was measured (Shchekin *et al.*, 2002).
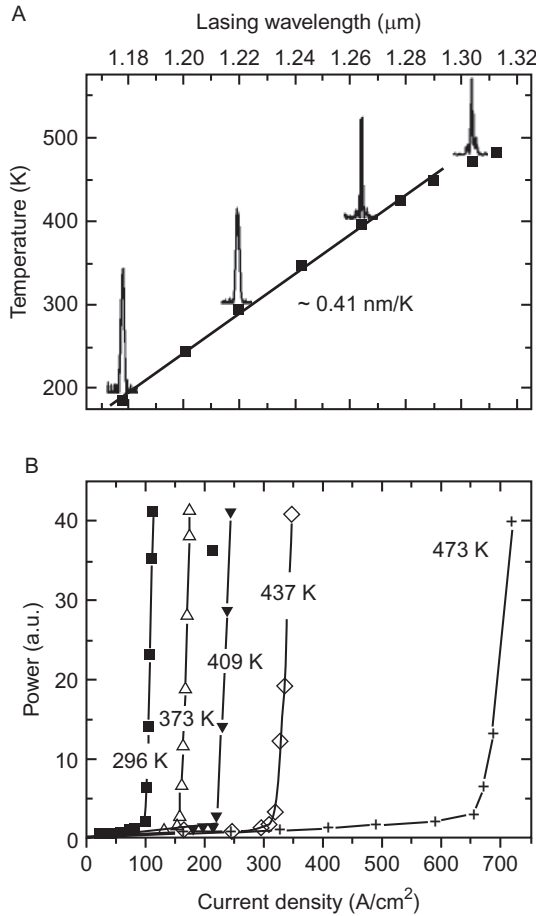
**FIGURE 10.5**   Truncated QD laser characteristics as a function of temperature: (A) ground-state lasing wavelength and corresponding spectra and (B) power–current characteristics at pulse excitation for 5.15-mm long laser diode. Adapted from Tokranov et al. (2003).

Based on a similar technology, Ishida et al. (2007) have been able to demonstrate temperature-insensitive 10Gb/s operation from 20 to 90°C for a directly modulated QD laser. The device utilized a high-modal-gain active region with 10-layer stacking of high-density QDs and p-type modulation doping. Figure 10.7 shows that the device maintains a clear eye opening, average output power, and extinction ratio over a broad temperature range without the need for current adjustments, thereby eliminating the need for corrective circuitry. Research at QD Laser, Inc., Fujitsu Laboratories and the University of Tokyo have reported on a
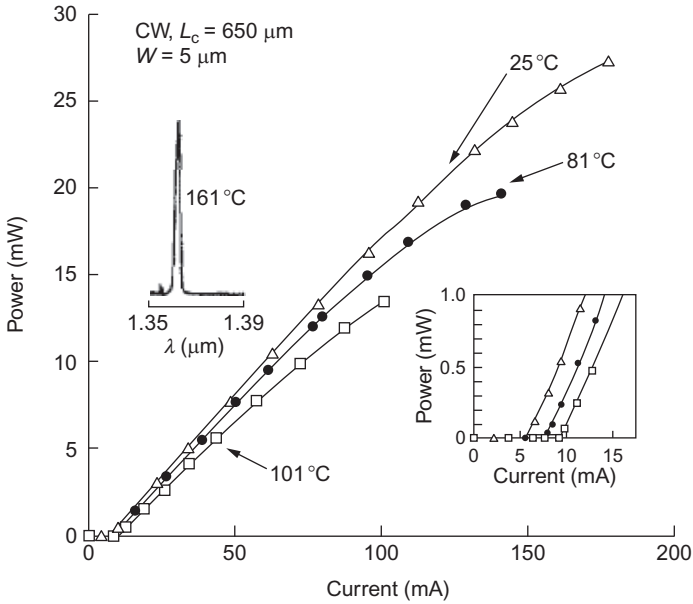
**FIGURE 10.6**   Light against current characteristics measured under CW operation (p-up-mounting) for three different temperatures Threshold currents are 5.7 mA at 25 °C, 7.6 mA at 81 °C, and 9.3 mA at 101 °C Inset: Lasing spectra at 161 °C. Adapted from Shchekin *et al.* (2002).
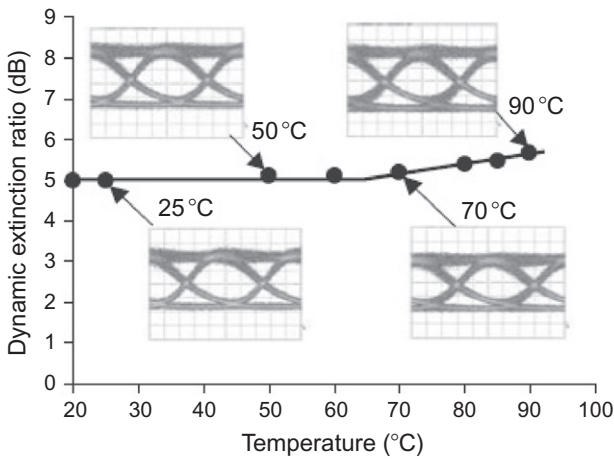


**FIGURE 10.7**   Temperature dependence of dynamic extinction ratio under 10 Gbits modulation (NRZ, $2^{31}-1$ PRBS). Modulation current: 25.5 mA (fixed). Bias current: 23.4 mA (fixed). Insets: Observed eye patterns at each temperature. Adapted from Ishida *et al.* (2007).
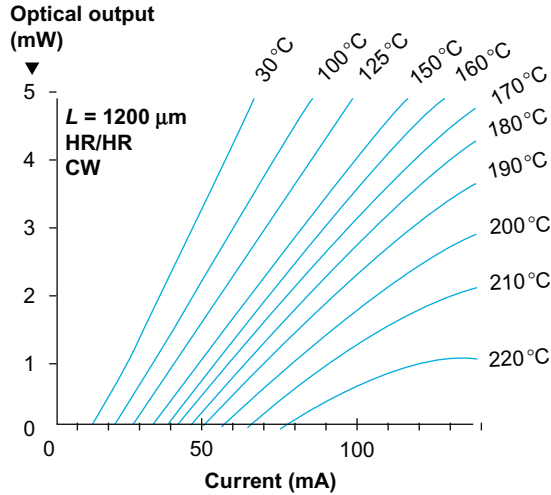
**FIGURE 10.8**    Light–output characteristics as a function of temperature for a 1.2-mm-cavity length quantum dot laser. Adapted from QD Laser Inc. (2011).

1.2-mm HR/HR-coated QD laser that operates up to 220°C, where it emits a CW output of 1 mW as shown in Fig. 10.8. This feat makes it usable in extreme environments such as those encountered deep underground in oil and gas drilling. Gain at such high temperatures was achieved by suppressing indium out-diffusion during the QD growth by molecular-beam epitaxy (QD Laser Inc., 2011). The optimized device consisted of eight-stacked layers, had a high dot density of $5.9 \times 10^{10} \mathrm{cm}^{-2}$ in each stacked layer, and included partially p-doped GaAs barriers. In addition, because the ground state and first excited state were separated by a large amount (80 meV), excited state lasing at very high temperatures was suppressed. Between 30 and 200°C, the laser has an impressive $T_0$ of 130 K.

## 3. THE LINEWIDTH ENHANCEMENT FACTOR IN QUANTUM DOT LASERS

The linewidth enhancement factor ($\alpha_H$-factor) is commonly used to distinguish the behavior of SLs with respect to other types of lasers (Henry, 1982) and influences several fundamental aspects such as the linewidth (Henry, 1982; Su *et al.*, 2004), the chirp under modulation (Petermann, 1991), the laser's behavior under optical feedback (Grillot *et al.*, 2008a; Su *et al.*, 2003), as well as the occurrence of the filamentation in broad-area lasers (Marciante and Agrawal, 1996). The $\alpha_H$-factor is usually defined as

the coupling between the phase and the amplitude of the electric field such as (Henry, 1982):

$$\alpha_{\mathrm{H}} = -\frac{4\pi}{\lambda}\frac{\mathrm{d}n/\mathrm{d}N}{\mathrm{d}g/\mathrm{d}N} = -\frac{4\pi\Gamma}{\lambda}\frac{\mathrm{d}n/\mathrm{d}N}{\mathrm{d}G_{\mathrm{net}}/\mathrm{d}N} \qquad (10.2)$$

where $\lambda$ is the lasing wavelength, $N$ the carrier density, $g$ is the material gain, $\Gamma$ the optical confinement factor, and $G_{\mathrm{net}} = \Gamma_g - \alpha_i$ the net modal gain with $\alpha_i$ the internal loss coefficient. The $\alpha_{\mathrm{H}}$-factor depends on the ratio of the evolution of the refractive index $n$ with the carrier density $N$ to that of the differential gain $\mathrm{d}g/\mathrm{d}N$. Several different techniques have been proposed to measure the $\alpha_{\mathrm{H}}$-factor, without any rigorous comparison between the results achieved (Giuliani *et al.*, 2007; Osinski and Buus, 1987). Also, it should be stressed that the number of the proposed measuring methods has kept increasing while novel types of SLs such as those based on QD have arisen, for which the determination of the $\alpha_{\mathrm{H}}$-factor may be particularly critical (Grillot *et al.*, 2008b). Several models early on predicted a near-zero $\alpha_{\mathrm{H}}$-factor due to the discrete density of states (Bimberg *et al.*, 1997). Several groups have reported different values of the $\alpha_{\mathrm{H}}$-factor associated with various techniques: for instance, a negative value to about 2 has been measured (Newell *et al.*, 1999; Uskov *et al.*, 2004). On the other hand, an $\alpha_{\mathrm{H}}$-factor as low as 0.1 has been determined in single-stack QD lasers (Smowton *et al.*, 2003), while a minimum of about 1.0 has been observed in a multi-stack sample (Ukhanov, 2004). A comparative study of the linewidth enhancement factor in p-doped and undoped QD lasers based on a combination of theoretical and experimental investigations was carried out to elucidate the influence of the p-type dopants. It was found that the p-doped QD lasers exhibited a lower linewidth enhancement factor near threshold relative to the undoped QD lasers. (Kim *et al.*, 2006a,b). This observation was attributed to the reduced transparency carrier density enabled by the combination of p-type modulation doping and a low density of states semiconductor system.

The section aims to investigate the influence of the nonlinear effects related to the gain compression and its consequences on the above-threshold $\alpha_{\mathrm{H}}$-factor both for QW and QD devices. The first part starts by giving an overview of the most common experimental techniques (below and above threshold) used for determining the $\alpha_{\mathrm{H}}$-factor. Then, the second part concentrates on analytical issues including nonlinear effects to model the behavior of the $\alpha_{\mathrm{H}}$-factor above the laser's threshold. Especially, in the case of QD lasers, the model not only explains the dependence of the $\alpha_{\mathrm{H}}$-factor with the injected current but also the fact that the $\alpha_{\mathrm{H}}$-factor can balloon to giant values as the lower energy states of the QDs are saturated. After this dramatic increase, the $\alpha_{\mathrm{H}}$-factor may even plummet to negative values. The increase of the $\alpha_{\mathrm{H}}$-factor in a QD laser with the

pump current is attributed to the enhancement of the gain compression through the gain saturation with the carrier density in QDs. This section potentially identifies ways to control and exploit the dramatic changes occurring in the $\alpha_H$-factor so as to achieve a QD laser with a controllable and highly variable $\alpha_H$-factor, as was demonstrated by Goulding *et al.* in a QD semiconductor optical amplifier (Goulding *et al.*, 2007).

## 3.1. Major experimental techniques for measuring the $\alpha_H$-factor

In most cases, the $\alpha_H$-factor is evaluated by using the so-called Hakki–Paoli sub-threshold method, which relies on direct measurement of the refractive index change and the differential gain as the carrier density is varied by slightly changing the current of an SL (Hakki and Paoli, 1975; Henning and Collins, 1983). This method applicable only below threshold gives the material $\alpha_H$-factor and does not correspond to an actual lasing condition. As a consequence, it makes more sense to determine the $\alpha_H$-factor above the laser's threshold. Thus, relevant aspects such as the high-power behavior of the $\alpha_H$-factor due to nonlinear effects and the consequences on the adiabatic chirp can be taken into account. Thus, the $\alpha_H$-factor appears as an optical power-dependent parameter strongly influenced by nonlinear gain and/or carrier-heating effects (Agrawal, 1990). Such power dependence is particularly strengthened in QD lasers in which the lasing wavelength can switch from the GS to the ES as the injected current increases. This accumulation of carriers in the ES arises even though lasing in the GS is still occurring and therefore increases the effective $\alpha_H$-factor of the GS transition introducing a nonlinear dependence with the injected current (Grillot *et al.*, 2008b). Among the above-threshold techniques used for measuring the $\alpha_H$-factor, the linewidth method relies on the measurement of SL's linewidth, and on fitting the results to known SL's parameters, so that the $\alpha_H$-factor can be extracted by applying Eq. (26) from Henry (1982). Taking into account that the laser's linewidth exhibits different slopes below and above threshold, a method to determine the $\alpha_H$-factor in a single-mode case was also proposed in Toffano *et al.* (1992). Finally, the modified linewidth method relies on the measurement of SL's linewidth as a function of emitted power under and above the laser's threshold, and the ratio of the slopes of the curves linewidth as a function of the inverse power gives directly the $\alpha_H$-factor value (Villafranca *et al.*, 2005). Such a method has been recently generalized to FP SLs (Villafranca *et al.*, 2009). Those methods based on the SL's linewidth both require a thorough characterization of the specific device under test and suffer from a poor accuracy due to the complex dependence of the laser's linewidth on several parameters. Two other possibilities for measuring the above-threshold $\alpha_H$-factor rely on injection locking or on optical feedback techniques. On one hand, light

from a master SL is injected into the slave SL causing locking of the slave optical frequency to that of the master. The locking region is characterized in terms of the injected power level and frequency detuning, showing an asymmetry in frequency due to the nonzero $\alpha_H$-factor (Hui *et al.*, 1990; Liu *et al.*, 2001). An accurate measurement of the effective injection level is generally difficult because there always exists a mode profile mismatch between the master beam projected onto the slave laser facet and the slave-guided mode. Such mismatch can reduce the effective injection to a value that is 10–50% of the total facet power meaning that the accuracy is limited. On the other hand, the optical feedback method is based on the self-mixing interferometry configuration and, according to the Lang–Kobayashi theory, the $\alpha_H$-factor is determined from the measurement of specific parameters of the resulting interferometric waveform. Unlike the injection-locking method, the accuracy appears better as long as the knowledge of the effective feedback level is not required (Yu *et al.*, 2004). Also it is important to stress that a theoretical and experimental investigation of reflectograms obtained for a DFB SL using a phase-controlled high-resolution optical low-coherence reflectometer (OLCR) was carried out in Palavicini *et al.* (2003). Among other results, it is shown that the $\alpha_H$-factor can be directly deduced from the OLCR measurements. Finally, the determination of the $\alpha_H$-factor can be conducted through high-frequency techniques. On one hand, the SL current modulation generates both amplitude (AM) and optical frequency (FM) modulation (Harder *et al.*, 1983). The ratio of the FM over AM components gives a direct measurement of the $\alpha_H$-factor (Harder *et al.*, 1983; Kruger and Kruger, 1995; Shimpe *et al.*, 1986; Zhang *et al.*, 2007). The AM term can be measured by direct detection via a high-speed photodiode, while the FM term is related to sidebands intensity that can be measured using a high-resolution scanning FP filter. Although the FM/AM method requires modulation well above the SL's relaxation frequency, this technique gives the device $\alpha_H$-factor under direct modulation. On the other hand, the fiber transfer function method originally proposed for electroabsorption modulators (EAMs) (Devaux *et al.*, 1993) exploits the interaction between the chirp of a high-frequency-modulated SL and the chromatic dispersion of an optical fiber, which produces a series of minima in the amplitude transfer function versus modulation frequency. Such a technique has then been generalized to diode lasers by introducing the adiabatic term as shown in references (Royset *et al.*, 1994; Srinivasan and Cartledge, 1995) and by fitting the measured transfer function, the $\alpha_H$-factor can be retrieved. This method has been shown to be reliable as long as precise measurement of fiber dispersion is made and as long as the power along the fiber span is kept sufficiently low to avoid nonlinear effects. Compared to the FM/AM technique, the main disadvantage of such a method is that several fitting parameters have to be determined to access the $\alpha_H$-factor. Another

important issue concerns the determination of the sign of the $\alpha_H$-factor, which is of first importance for many applications requiring ultra-low laser linewidth such as on-chip pulse compression, chirp compensation, or for EAMs. Among all the techniques explained above, only the fiber transfer function method can give the phase and then the sign of the $\alpha_H$-factor. Recently, another method using an optical discriminator based on a tunable Mach–Zehnder (MZ) interferometer has been used to extract AM and FM responses both in amplitude and in phase as well as the $\alpha_H$-factor (Provost and Grillot, 2011). Although both Michelson and MZ interferometers have already been used in the past to measure the SL's FM responses (Goobar *et al.*, 1988; Sorin *et al.*, 1992; Vodhanel and Tsuji, 1988; Wellford and Alexander, 1985), the proposed method not only allows to evaluate the $\alpha_H$-factor but also the adiabatic chirp and the thermal effects. As discussed in Provost and Grillot (2011), the proposed technique is also much quicker as compared to the fiber transfer one and can easily be converted to a large-signal analysis configuration (Saunders *et al.*, 1994).

## 3.2. Models for analyzing the above-threshold $\alpha_H$-factor

### 3.2.1. QW lasers

In QW lasers, which are made from a nearly homogeneously broadened gain medium, the carrier density and distribution are clamped at threshold. As a result, the change of the $\alpha_H$-factor is mostly due to the decrease of the differential gain from gain compression and can be expressed in the simplest case as follows (Su *et al.*, 2005):

$$\alpha_H(P) = \alpha_{H0}(1 + \varepsilon_P P) \qquad (10.3)$$

where $\alpha_{H0}$ is the $\alpha_H$-factor at threshold and $\varepsilon_P$ the gain compression coefficient related to the output power $P$. Let us stress that sometimes it is also useful to express the gain compression in terms of a saturation power such as $\varepsilon_P P = P/P_{sat}$. The saturated power $P_{sat}$ means that at this level of output power, nonlinear effects start to be significant. Since the carrier distribution is clamped, $\alpha_{H0}$ itself does not change that much as the output power increases. As an example, Fig. 10.9 shows the measured $\alpha_H$-factor versus the output power for a 300-µm-long AR/HR-coated DFB laser made from six compressively strained QW layers. The threshold current is ~8mA at room temperature for the QW DFB device. Black squares correspond to experimental data. As described by Eq. (10.3) for the powers studied, the effective $\alpha_H$-factor linearly increases with the output power to about 4.3 at 10mW. By curved-fitting the data, the $\alpha_H$-factor at threshold is about 4, while the gain compression coefficient equals $\sim 3 \times 10^{-2} \text{mW}^{-1}$. Compared to QD lasers, such a value of the gain
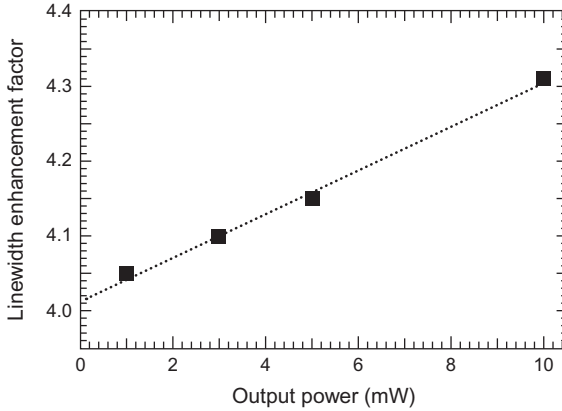
**FIGURE 10.9**  The effective $\alpha_H$-factor as a function of the output power for a QW DFB laser. Adapted from Grillot *et al.* (2008b).

compression coefficient is much smaller leading to a higher saturation power, which lowers the enhancement of the effective $\alpha_H$-factor with power.

The response of the semiconductor active medium to the intracavity optical field is governed by a set of density-matrix equations, which take into account intraband relaxation of charge carriers within the conduction and valence bands as well as the relaxation of the induced polarization (Agrawal, 1990). Since the three relaxation times are much shorter than the photon and carrier lifetimes, the medium is often assumed to respond instantaneously to the intracavity field. The steady-state solution of the density-matrix equations in that case can be used to obtain the carrier-induced change in the susceptibility, which consists of a linear part and a nonlinear part. As a result, another expression giving the intensity dependence of the $\alpha_H$-factor through the implementation of the intraband relaxation effects responsible for nonlinear gain and index changes can be expressed as follows (Agrawal, 1990):

$$\alpha_H(P) = \alpha_0(1 + \varepsilon_E P)^{1/2} + \beta \varepsilon_P P \frac{(1 + \varepsilon_P P)}{2 + \varepsilon_P P} \tag{10.4}$$

with $\beta$ the parameter related to the slope of the linear gain which controls the nonlinear phase change defined such as:

$$\beta(\omega) = \frac{-2(\omega - \omega_P)}{\tau_{in}\Delta\omega_g^2} \tag{10.5}$$

with $\tau_{in}$ the intraband relaxation time, $\omega$ the lasing frequency, $\omega_P$ the gain-peak frequency, and $\Delta\omega_g$ the gain bandwidth. The situation for
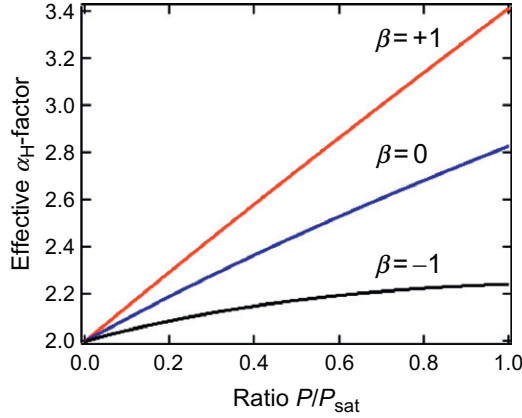
**FIGURE 10.10**   Calculated effective $\alpha_H$-factor as a function of the ratio $P/P_{sat}$ for different values of coefficient $\beta=-1$, 0, $+1$.

which $\beta=0$ corresponds to an oscillation purely located at the gain peak which is the situation encountered for an FP laser. However, $\beta$ can be a nonzero parameter for DFB lasers, which can operate at wavelengths away from the gain peak as a result of the feedback provided by the built-in grating. Consequently, $\beta$ can be positive or negative depending on whether the DFB laser operates on the red or the blue side of the gain peak. Typical values of $\beta$ are expected to be such that $|\beta|< 1$. Figure 10.10 shows a simulation of the effective $\alpha_H$-factor as a function of the ratio $P/P_{sat}$ for different values of coefficient $\beta=-1$, 0, $+1$. For DFB lasers negatively detuned ($\omega<\omega_P$), the second part of Eq. (10.4) usually remains small enough to be neglected and the power dependence of the effective $\alpha_H$-factor is roughly linear as previously shown in Fig. 10.9. However, for DFB lasers positively detuned ($\omega>\omega_P$), some nonlinearities could arise in the power dependence of the effective $\alpha_H$-factor leading to either a saturation or even to a strong roll-off when large nonlinear effects are considered.

### 3.2.2. QD lasers
In QD lasers, the carrier density and distribution are not clearly clamped at threshold. Based on this fact, the lasing wavelength can switch from GS to ES as the current injection increases meaning that a carrier accumulation occurs in the ES even though lasing in the GS is still occurring. The filling of the ES inevitably increases the $\alpha_H$-factor of the GS and introduces an additional dependence with the injected current. Thus taking into

account the gain variation at the GS and at the ES, the index change at the GS wavelength can be written as follows:

$$\delta n = \sum_{k=\text{GS,ES}} \alpha_k \delta g_k \tag{10.6}$$

with $k$ being the index of summation for the GS and ES, respectively. Equation (10.6) can be expressed as follows:

$$\delta n = \left( \alpha_{\text{ES}} \frac{a_{\text{ES}}}{a_{\text{GS}}} + \alpha_{\text{GS}} \right) \delta g_{\text{GS}} = \alpha_H \delta g \tag{10.7}$$

In Eq. (10.7), $\delta g$ and $\delta n$ are the changes of the gain and refractive index at the GS, respectively, $\alpha_H$ is the GS linewidth enhancement factor actually measured in the device, $a_{\text{ES}}$ and $a_{\text{GS}}$ are the differential gain values at the ES and at the GS, respectively, $\alpha_{\text{ES}}$ describes the change of the GS index caused by the ES gain and $\alpha_{\text{GS}}$ is related to the GS index change caused by the GS gain variation. When the laser operates above threshold, $\alpha_{\text{GS}}$ keeps increasing with $\alpha_{\text{GS}}(1+\varepsilon_P P)$ as previously shown for the case of QW devices.

The gain saturation in a QD media can be described by the following equation (Su *et al.*, 2005):

$$g_{\text{GS}} = g_{\max}\left[1 - \exp\left(-\ln(2)\left(\frac{N}{N_{\text{tr}}} - 1\right)\right)\right] \tag{10.8}$$

with $N$ the carrier density and $N_{\text{tr}}$ the transparency carrier density. When the laser operates above threshold, the differential gain for the GS lasing is defined as follows:

$$a_{\text{GS}} = \frac{dg_{\text{GS}}}{dN} = \frac{\ln(2)}{N_{\text{tr}}}(g_{\max} - g_{\text{GS}}) \tag{10.9}$$

with $g_{\max}$ the GS maximum modal gain and $g_{\text{GS}} = g_{\text{th}}(1+\varepsilon_P P)$ the uncompressed material gain increasing with the output power, $g_{\text{th}}$ being the GS modal gain at threshold. Equation (10.9) leads to:

$$a_{\text{GS}} = a_0\left(1 - \left(\frac{g_{\text{th}}}{g_{\max} - g_{\text{th}}}\right)\varepsilon_P P\right) \tag{10.10}$$

with $a_0$ the differential gain at threshold. Then using Eqs. (10.3), (10.7), and (10.10), the $\alpha_H$-factor can be analytically written as:

$$\alpha_H(P) = \alpha_{\text{GS}}(1 + \varepsilon_P P) + \frac{\alpha_{\text{ES}}(a_{\text{ES}}/a_0)}{1 - \left(\frac{g_{\text{th}}}{g_{\max} - g_{\text{th}}}\right)\varepsilon_P P} \tag{10.11}$$

The first term in Eq. (10.11) denotes the gain compression effect at the GS (similar to QW lasers when coefficient $\beta$ is negligible), while the second is the contribution from the carrier filling in the ES that is related to the gain saturation in the GS. For the case of strong gain saturation or lasing on the peak of the ground-state gain, Eq. (10.11) can be reduced to:

$$\alpha_H(P) = \frac{\alpha_{ES}(a_{ES}/a_0)}{1 - \left(\frac{g_{th}}{g_{max}-g_{th}}\right)\varepsilon_P P} \tag{10.12}$$

It is noted that previous work has also confirmed the increase in the $\alpha_H$-factor with injection (Melnik and Huyet, 2006). By comparing three techniques commonly used to measure the $\alpha_H$-factor of QD lasers, their analysis, which is based on QD rate equations and incorporates both the finite capture time of carriers into the dots and plasma effects (Hegarty et al., 2005; Uskov et al., 2004), has shown that each of the three techniques gives a different value for the measured $\alpha_H$-factor.

Figure 10.11 from Melnik and Huyet (2006) shows that the $\alpha_H$-factor depends on the nonresonant carrier density and that this contribution becomes more important near full inversion as shown. Close to full inversion it is shown that the dot occupation probability saturates, but
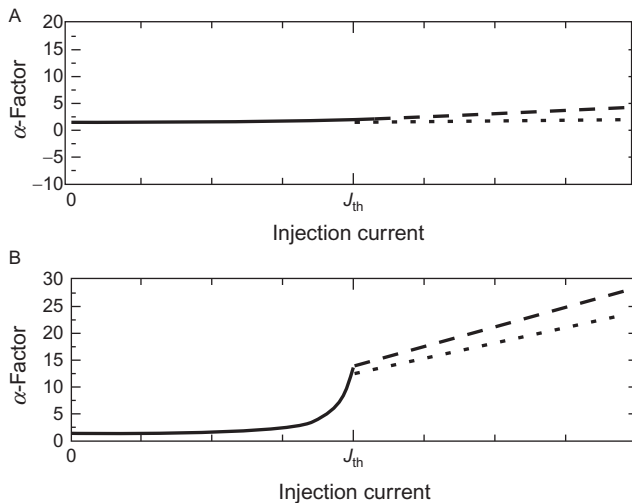


FIGURE 10.11  Values of the $\alpha$-factor calculated by the following techniques: solid line is the ASE method, dashed line is the FM/AM method, and dotted line is the linewidth method. (A) Laser operates for nonsaturated dots. (B) Laser operates close to full inversion. For the nonsaturated operating point (A) the $\alpha$-factor does not show strong dependence on the injection current. This is not the case for operation close to full inversion (B). Adapted from Melnik and Huyet (2006).
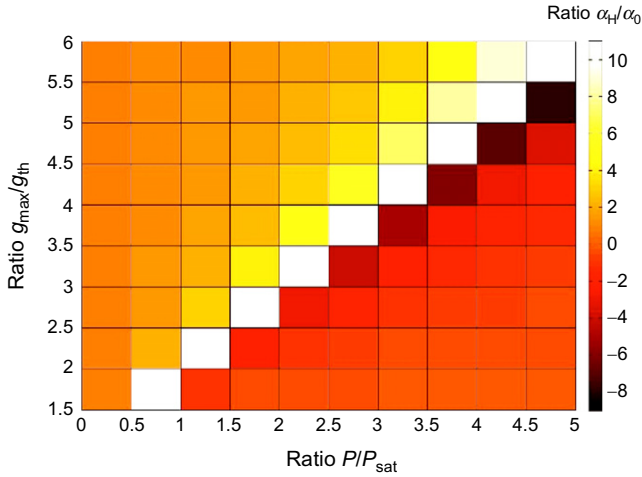
**FIGURE 10.12** Stability map based for the normalized linewidth enhancement factor $\alpha_H/\alpha_0$ in the ($P/P_{sat}$, $g_{max}/g_{th}$) plane. Adapted from Grillot *et al.* (2008b).

the carrier density in the wetting layer continues to increase with current, leading to a dramatic increase in the $\alpha_H$-factor.

In Fig. 10.12, the normalized $\alpha_H$-factor $\alpha_H/\alpha_0$ with $\alpha_0 = \alpha_{ES}(a_{ES}/a_0)$ is calculated through Eq. (10.11) and represented in the ($X,Y$) plane with $X = P/P_{sat}$ and $Y = g_{max}/g_{th}$. This graph serves as a stability map and simply shows that a larger maximum gain is absolutely required for a lower and stable $\alpha_H/\alpha_0$ ratio. For instance, let us consider the situation for which $g_{max} = 3g_{th}$: at low output powers, that is, $P < P_{sat}$, the normalized $\alpha_H$-factor remains constant ($\alpha_H/\alpha_0 \sim 3$) since the gain compression is negligible. As the output power approaches and goes beyond $P_{sat}$, the ratio $\alpha_H/\alpha_0$ is increased. Gain compression effects lead to an enhancement of the normalized $\alpha_H$-factor, which can go up to 10 for $P \approx 2P_{sat}$ level of injection for which the ES occurs.

Assuming that $g_{max} = 5g_{th}$, Fig. 10.12 shows that the effects of gain compression are significantly attenuated since the ratio $\alpha_H/\alpha_0$ remains relatively constant over a wider range of output power. The level at which gain compression starts being critical is now shifted to $P \approx 3P_{sat}$ instead of $P \approx P_{sat}$. It is also important to note that at a certain level of injection, the normalized GS $\alpha_H$-factor can even become negative. This effect has been experimentally reported in Dagens *et al.* (2005) and occurs when the GS gain collapses, for example, when ES lasing occurs.

In Fig. 10.13, the calculated GS $\alpha_H$-factor (black dots) of the QD laser from Dagens *et al.* (2005) is depicted as a function of the bias current. The red stars appearing in Fig. 10.13 correspond to data measurements from
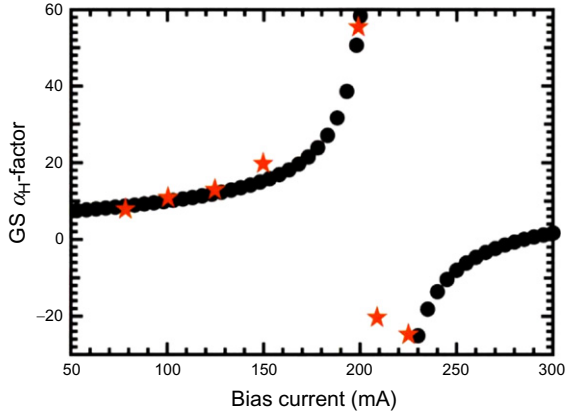
**FIGURE 10.13** Calculated GS $\alpha_H$-factor for a QD laser versus the bias current (black dots). Superimposed red stars correspond to experimental data. Adapted from Grillot *et al.* (2008b).

Dagens *et al.* (2005) which have been obtained via the AM/FM technique (Provost and Grillot, 2011). Figure 10.13 shows a qualitative agreement between the calculated values and the values experimentally obtained. As expected, the GS $\alpha_H$-factor increases with the injected current due to the filling of the excited states as well as carrier filling of the nonlasing states (higher lying energy levels such as the wetting layer). Although the $\alpha_H$-factor is lowered at smaller output powers, its increase with bias current stays relatively limited as long as the bias current remains lower than 150mA, for example, such that $P < P_{sat}$. Beyond $P_{sat}$, compression effects become significant, and the $\alpha_H$-factor reaches a maximum of 57 at 200mA before collapsing to negative values. As previously mentioned, the collapse in the $\alpha_H$-factor is attributed to the occurrence of the ES as well as to the complete filling of the available GS states. In other words, as the ES stimulated emission requires more carriers, it affects the carrier density in the GS, which is significantly reduced. As a result, the GS $\alpha_H$-factor variations from 57 down to $-30$ may be explained through a modification of the carrier dynamics such as the carrier transport time including the capture into the GS. This latter is known to affect the modulation properties of high-speed lasers via a modification of the differential gain. These results are of significant importance because they show that the $\alpha_H$-factor can be controlled by properly choosing the ratio $g_{max}/g_{th}$: the lower the $g_{th}$, the higher the $g_{max}$, and the smaller the line-width enhancement factor. A high maximum gain can be obtained by optimizing the number of QD layers in the laser structure while gain at threshold is directly linked to the internal and mirror losses. Both $g_{th}$ and

$g_{max}$ should be considered simultaneously so as to properly design a laser with a high differential gain and limited gain compression effects. The $g_{max}/g_{th}$ ratio is definitely the key point in order to obtain a lower $\alpha_H$-factor for direct modulation in QD and QDash lasers. Other applications could also be considered such as on-chip chirp compensation or pulse compression for which a laser section that has a negative $\alpha_H$-factor could compensate the positive chirp that is typically encountered in the pulses of an SL. Indeed, it is well known that in case of directly modulated lasers, the interaction of the $\alpha_H$-factor with the chromatic dispersion of standard single-mode fibers (SMF) set the limit of the maximum attainable transmission distance for a given bit rate. A laser with a negative $\alpha_H$-factor could counteract the positive chirp of optical fibers, allowing signals to travel with less degradation. This last point is of first importance for many applications in optical telecommunications since ultrashort laser pulses spread out due to the dispersion of the waveguiding material.

## 4. QD DISTRIBUTED FEEDBACK LASERS

Since the invention of the laser, spectral purity of the lasing mode has always been of central interest. Although gas and solid-state lasers typically have a narrower linewidth than SLs, the former are inferior when their cost, size, and reliability are considered. Much research has been conducted on narrow linewidth SLs. Different device designs, such as the external cavity configuration (Fleming and Mooradian, 1981; Matthews *et al.*, 1985; Patzak, *et al.*, 1983) and chirped grating DFBs (Okai, 1994; Okai *et al.*, 1994), have been proposed to achieve narrow linewidth. Meanwhile, new semiconductor materials, for instance, strained QWs (Takano *et al.*, 1989) and finally QDs, have been proposed for narrow linewidth operation because of their low internal loss and small linewidth enhancement factor. Therefore, studies of the linewidth of QD lasers are important. In real-world applications, single-mode DFB lasers at 1.3 μm with narrow spectral linewidth are essential for various applications, such as coherent sources and local oscillators for communication systems (Agrawal, 2002).

As discussed previously, 1.3-μm devices based on InAs/InGaAs DWELL technology have become promising alternatives to lasers built on InP-based materials, due to their low substrate cost, excellent temperature performance, low-threshold current, and small linewidth enhancement factor, $\alpha_H$. Theoretical calculations also show that the population inversion factor, $n_{sp}=(1/1-\exp(E_{21}-\Delta E_F/k_B T))$, where $E_{21}$ is the energy separation of the bands and $\Delta E_F$ is the difference in their associated Fermi levels, is lower in QDs than in QWs (Berg and Mork, 2003). These advantages of QDs over QWs suggest that QD lasers can have narrow linewidth, considering the following equation:

$$\Delta v = \frac{\Gamma g_{\text{th}} v_{\text{g}} \alpha_{\text{m}} hv}{4\pi P_0} n_{\text{sp}} \left(1 + \alpha_{\text{H}}^2\right) \tag{10.13}$$

where $\Delta v$ is the linewidth, $g_{\text{th}}$ is the threshold gain, $P_0$ is the optical output power, $\Gamma$ is the confinement factor, $v_{\text{g}}$ is the group velocity, $\alpha_{\text{m}}$ is the mirror loss, and $hv$ is the photon density (Coldren and Corzine, 1995).

Theoretically, a narrow linewidth is always obtained by increasing the laser power as indicated by Eq. (10.13). In real cases, however, the minimum achievable linewidth is typically limited by linewidth rebroadening or a floor due to mode instability (Olesen *et al.*, 1992), the existence of side modes (Pan *et al.*, 1991), spatial-hole burning (Okai, 1994; Wenzel *et al.*, 1991), or gain compression (Agrawal *et al.*, 1992; Girardin *et al.*, 1996). The first three of these effects are mostly related to the device structure and can be minimized or eliminated by optimizing the device design. However, gain compression is fundamentally related to the timescales for the carrier equilibrium dynamics in the semiconductor gain media and is enhanced in QD gain media. Therefore, understanding the trade-offs involved with introducing QDs into a laser intended for narrow linewidth operation is essential.

## 4.1. Narrow linewidth devices

The linewidth of QD DFBs with different gain offsets and a commercial 1.3-µm index-coupled QW DFB from Mitsubishi, Inc. are studied in this section. The QD DFBs are complex coupled to a lateral chromium grating alongside the ridge waveguide laser cavity (Su *et al.*, 2003; Zhang *et al.*, 2003). The gain offset is defined as the difference between the DFB wavelength and the gain-peak wavelength. The cavity length of the QD and QW DFBs is 300 µm. The static characteristics of the devices are presented in Table 10.1. The optical spectra at 10 mA injection current are shown in Fig. 10.14.

**TABLE 10.1**  The Performance of QD DFBs A, B, and C and the Commercial QW DFB at Room Temperature

| Device # | A | B | C | QW DFB |
|---|---|---|---|---|
| $I_{\text{th}}$ (mA) | 3 | 5 | 6 | 7.8 |
| Slope efficiency $\eta$ (mW/mA) | 0.16 | 0.20 | 0.12 | 0.2 |
| $\lambda$ at 10 mA (nm) | 1297 | 1309 | 1324 | 1305 |
| Gain peak at 10 mA (nm) | 1309 | 1309 | 1305 | N.A. |
| SMSR at 10 mA (dB) | 57 | 48 | 41 | 44.6 |
| SMSR at 45 mA (dB) | 56 | 53 | 45 | 50 |
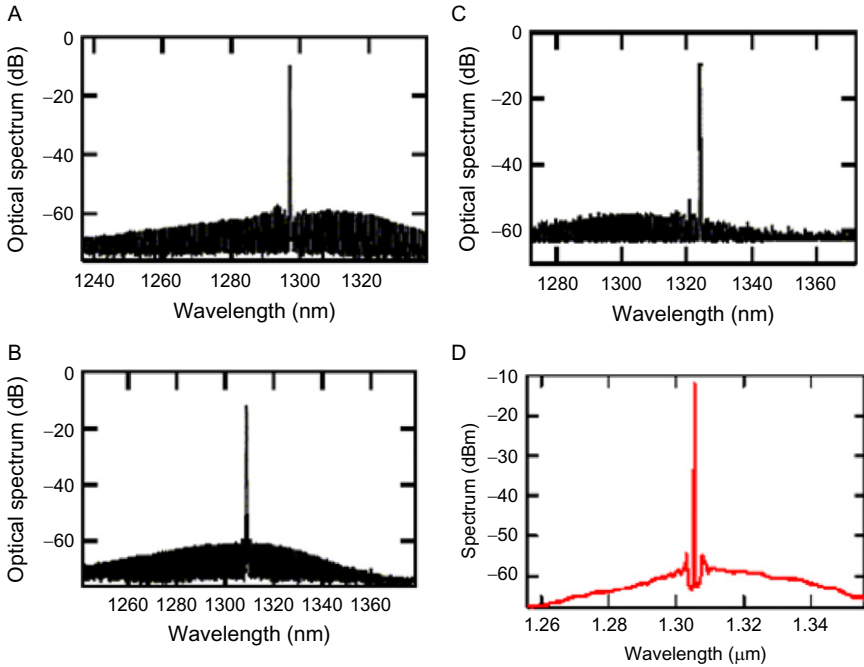
**FIGURE 10.14**    (A), (B), and (C) The spectra of devices A, B, and C at 10mA, respectively. (D) The spectrum of the commercial QW DFB at 10mA. Adapted from Su *et al.* (2004).

While a stop band is clearly observed in the index-coupled QW DFB, this phenomenon is not seen in the QD DFBs due to the use of the lateral metal grating. The linewidth is measured with the self-homodyne technique (Okoshi *et al.*, 1980) using a fiber interferometer with a 3.5-μs delay. To avoid the external feedback into the DFBs, two cascaded isolators are applied for isolation better than 60dB. In addition, the fiber end in the coupling system is angle polished. The absence of sensitivity to external feedback is confirmed by the fact that the measured linewidth does not change even when the tilted angle of the coupling fiber is varied by about 3°.

Figure 10.15 shows the linewidths and side-mode suppression ratios (SMSR) of the three QD DFBs as a function of the optical output power. The linewidth–power product of devices A and B is about 0.8–1.2MHz mW for the output power less than 2mW, which is more than an order of magnitude smaller than the value of 16MHzmW measured in the commercial QW DFB at 2mW as shown in Fig. 10.16. In fact, the typical linewidth–power product in QW DFBs is tens of MHzmW depending on the cavity length (Coldren and Corzine, 1995). This result is physically consistent with the properties of the QD gain media discussed in
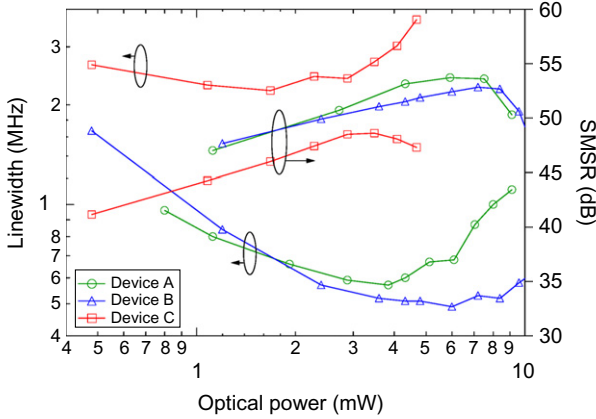
**FIGURE 10.15**    Linewidths and SMSRs of the three QD DFBs as a function of optical output power. Adapted from Su *et al.* (2004).
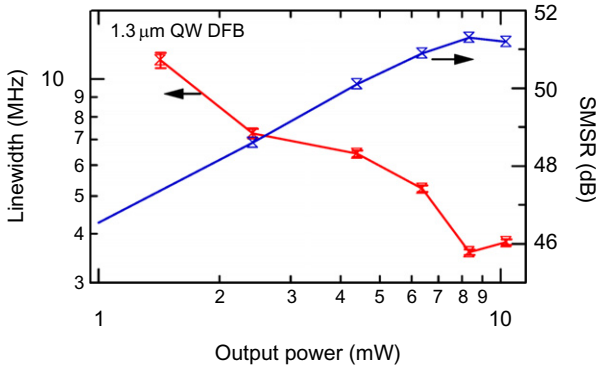


**FIGURE 10.16**    Linewidth and SMSR of a commercial 1.3-μm QW DFB.

Section 1, as well as the implementation of the loss-coupled grating, which reduces the adverse spatial-hole-burning effect, and the HR/HR coatings that lower the threshold gain. In device C, due to its larger gain offset and therefore larger $\alpha$, a wider linewidth at low power compared to devices A and B is observed. Further discussion of the linewidth rebroadening seen in the QD DFBs above 5mW output power is discussed elsewhere (Su *et al.*, 2004).

To understand the narrow linewidth of QD DFBs, the threshold modal gain, mirror loss and $n_{sp}(1+\alpha_H^2)$ can be estimated and compared to the values of typical QW DFBs. By knowing the internal loss, mirror loss and the slope efficiency of QD FPs fabricated on the same wafer as the QD

**TABLE 10.2**   Estimating the Figure of Merit for Narrow Linewidth in QD DFBs

Mirror loss: $\alpha_m = \frac{1}{2L} \ln\left(\frac{1}{R_1 R_2}\right) = 4.7 \, \text{cm}^{-1}$

Internal loss: $\alpha_i \approx 2 \, \text{cm}^{-1}$

Slope efficiency of QDFPs: $\eta_{FP} = 0.25 \, \text{mW/mA} \propto \frac{\alpha_m}{\alpha_i + \alpha_m}$

Slope efficiency of QD DFBs: $\eta_{DFB} = 0.14 \, \text{mW/mA} \propto \frac{\alpha_m}{\alpha_i + \alpha_m + \alpha_{grating}}$

DFB grating loss: $\alpha_{grating} = \frac{0.11}{0.14}(\alpha_i + \alpha_m) = 5.3 \, \text{cm}^{-1}$

DFB threshold modal gain: $\Gamma g_{th} = 12 \, \text{cm}^{-1}$

Output coupling factor: $F=1$, since most of the light is output from one facet

Linewidth–power product:

$(\Delta v)_{linewidth} P = \frac{\Gamma g_{th} v_g^2 F \alpha_m h v}{4\pi} n_{sp}(1 + \alpha^2) = 0.8 \, \text{MHz mW}$ at $1 \, \text{mW}$ output

$n_{sp}(1+\alpha^2) = 23$

DFBs, the threshold DFB modal gain and $n_{sp}(1+\alpha_H^2)$ are estimated to be $12 \, \text{cm}^{-1}$ and 23, respectively, from the fact that device A has a linewidth of 800 kHz at an output power of 1 mW (Table 10.2) (Su and Lester, 2005). For comparison, the values of $n_{sp}(1+\alpha_H^2)$ in QW gain media at similar modal gain values are three to four times higher (Zhao and Yariv, 1999). Since both a small $n_{sp}(1+\alpha_H^2)$ and a low-threshold gain are required for narrow linewidth operation, QDs are clearly advantageous compared QWs in this aspect.

## 4.2. QD DFBs for high external feedback resistance

A major problem with SLs, both FP and DFB types, is that they are highly sensitive to the laser light which reenters the laser cavity after being reflected by an external reflector. External optical feedback of the laser light usually causes instability of operation of a laser diode and generates excessive noise in optical communication systems (Petermann, 1991). A variety of optical elements, including lenses, fiber ends and integrated external cavities, can be the sources of unwanted optical feedback. For these reasons, costly and bulky optical isolators are typically required in most applications to protect SLs from optical feedback-induced noise.

One of the consequences of the external feedback on a laser is coherence collapse. When the external feedback exceeds a certain level, the laser becomes unstable and the coherence of the laser output is dramatically reduced. Initially, the linewidth versus external feedback level typically exhibits a narrowing as a function of feedback strength before the coherence collapse point, and then a dramatic linewidth rebroadening afterward (Petermann, 1991). Associated with this linewidth broadening is an increase in noise. Thus, avoiding coherence collapse is essential for

real-world applications. How exactly does the optical feedback process work? When external feedback is coupled into the laser cavity through the output facet, it causes a perturbation on the photon density. This perturbation leads to a fluctuation in the carrier density and thus the optical gain. The variation of gain itself changes the output power and consequently the external feedback strength. These processes form an intensity fluctuation loop that is effectively a self-intensity modulation and not sufficient to cause the complex dynamics of the laser system. On the other hand, since the fluctuations of optical index and gain are coupled by the linewidth enhancement factor, the external feedback can also introduce the phase fluctuation loop. The interaction of the intensity and phase loops essentially makes the dynamics of the laser system under external feedback very complex and results in system instability and even chaos. Thus, the motivation to investigate the behavior of QD DFBs under external feedback and demonstrate the improvement in their external feedback resistance is significant.

The setup for an optical feedback experiment is shown in Fig. 10.17. The laser output is coupled into a 3-dB optical fiber coupler. The feedback ratio is controlled by a variable optical attenuator, which gives attenuation from 1.5 to 80 dB. A film of 5000 Å Au is evaporated onto the flat fiber end of one arm of the coupler and functions as a reflective mirror. The distance between the laser and the external reflector is about 7 m. It is noteworthy that the critical external feedback level for coherence collapse does not depend on the distance between the external reflector and the output facet of the device. To avoid excess uncontrolled feedback, the coupling lens is AR coated and the fiber ends are angle polished in all connections. The external feedback ratio, which is defined as the ratio of the power reflected back to the laser facet and the single-facet output power of the device, is calculated as follows:
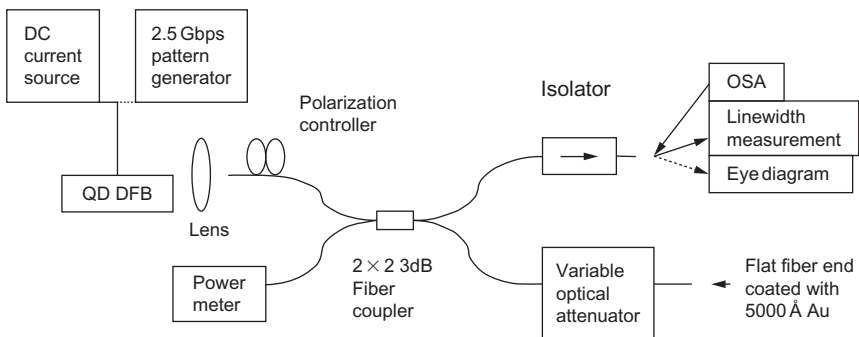


**FIGURE 10.17** Schematic of the experimental setup for external feedback studies on a QD DFB laser. Adapted from Su *et al.* (2003).

$$\Gamma_{dB} = P_1(dBm) - P_0(dBm) + C_{dB} \tag{10.14}$$

where the $P_1$ is the reading from the power meter in Fig. 10.17, $P_0$ is the output power of the laser, and $C_{dB}$ is the $-3.4\,dB$ coupling loss from the SL to the fiber. The coupling loss $C_{dB}$ is determined by the ratio between the total power after the 3-dB optical coupler (assumed lossless) and the output power directly measured at the facet of the DFB. The polarization controller is adjusted to obtain the maximum feedback effect to guarantee the same polarization of the feedback beam and the DFB cavity mode. The device is epoxy mounted on a heat sink and the temperature is controlled at 20°C. Optical spectra of the QD DFB under two different feedback levels are shown in Fig. 10.18. For a feedback ratio of $-14\,dB$, the lasing spectrum peak is slightly shifted. However, the spectral width is unchanged within the optical spectrum analyzer (OSA) resolution limit of 0.06 nm. For a higher resolution measurement, the linewidth of the DFB laser is determined by the self-homodyne technique with a fiber interferometer having a fixed delay of 3.5 µs. The linewidth with an external feedback ratio below $-60\,dB$ is 650 kHz at 5 mW output as shown in Fig. 10.19. As the feedback ratio increases, the linewidth narrows down quickly until the feedback ratio reaches $-14\,dB$, where the linewidth rebroadening occurs due to coherence collapse. However, the laser linewidth under $-14\,dB$ feedback is still less than 20 kHz, much less than the 650 kHz free-running linewidth. This result confirms the unchanged spectrum measured by the OSA. For comparison, the critical coherence collapse feedback ratio of an index-coupled QW DFB is typically between $-20$ and $-30\,dB$ (Grillot *et al.*, 2002; Petermann, 1991). For the 802.3ae 10 Gbps Ethernet standard, a laser must tolerate up to $-12\,dB$ feedback from
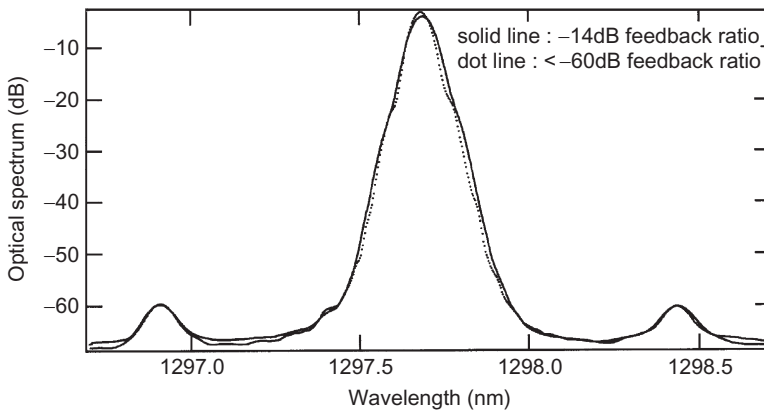


**FIGURE 10.18** The optical spectra of the QD DFB with $-14\,dB$ and less than $-60\,dB$ external feedback. No significant broadening is observed with the resolution of the optical spectrum analyzer to be 0.06 nm. Adapted from Su *et al.* (2003).
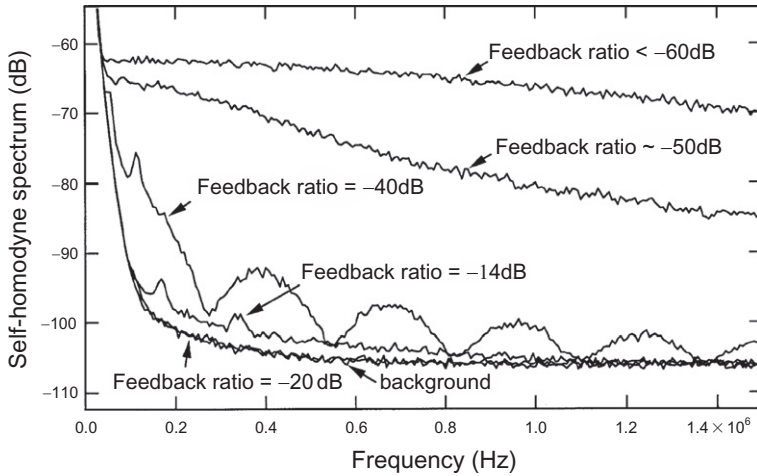
**FIGURE 10.19**    Self-homodyne spectra of the QD DFB under different external feedback strengths. Linewidth rebroadening occurs at −14 dB. Adapted from Su *et al*. (2003).

the network. For typical coupling losses of 4–6 dB in fiber-pigtailed lasers, a feedback ratio of −14 dB at the laser facet corresponds to −2 to −6 dB feedback from the system. Thus, the QD DFB is well suited to operate as an isolator-free light source in fiber-optic communication networks, as recently demonstrated by researchers in experiments conducted at 25 °C and data rates of 10 Gbps for 1.3 μm sources (Azouigui *et al*., 2011).

## 5. HIGH-SPEED PERFORMANCE OF QD LASERS

Advantages of directly modulated SLs for ultrafast communication applications have been thoroughly investigated over the past 25 years (Lau and Yariv, 1985; Nakahara *et al*., 2007; Weisser *et al*., 1994); however, achieving high-modulation bandwidths in such devices has been known to be limited by damping and the so-called *K*-factor (Olshansky *et al*., 1987). QD nanostructure-based lasers have been predicted to have superior dynamic properties compared to QW or bulk lasers making them potential candidates for high-speed applications (Bhattacharya *et al*., 2000; Klotzkin *et al*., 1998; Mao *et al*., 1997). This section reviews recent advancements and some of the techniques used to augment the high-speed performance of QD lasers.

    As previously mentioned, the predicted properties of QD nanostructure devices have been mostly verified on actual laser devices, including ultra-low transparency current density (Liu *et al*., 1999), and low-temperature dependence of threshold current density (Shchekin *et al*., 2002). In addition

to the advantages mentioned above, QD lasers have also been touted to exhibit an increased gain and differential gain (Asada *et al.*, 1986) as well as a reduced linewidth enhancement factor ($\alpha_H$-factor) (Newell *et al.*, 1999) which make them even more suitable for implementation in ultrafast and chirp-free optical transmitter modules. Compared to QW devices, potential for higher gain and differential gain in QD-based lasers would typically be expected to contribute to a larger modulation bandwidth (Lau and Yariv, 1985). Furthermore, QD nanostructure lasers are proven to possess a near-zero $\alpha_H$ at threshold, which based on theoretical premises would allow for chirp-free direct modulation (Newell *et al.*, 1999). After the successful demonstration of InAs and InGaAs QD nanostructures in 1994 (Kirstaedter *et al.*, 1994), developing high-speed QD lasers became a much more popular research topic, in particular since their lasing wavelength on GaAs covers 1.3μm, the zero-dispersion window of commercial communication systems (Mukai *et al.*, 1994). In spite of early predictions that QD lasers would exhibit speed enhancement, it is now well known that the modulation performance of these nanostructures is inherently limited by several factors. These range from the phonon bottleneck associated with relatively slow carrier-relaxation time (Urayama *et al.*, 2001), the inhomogeneous gain broadening (Bayer and Forchel, 2002), and hot carrier effects (Matthews *et al.*, 2002). As a result, the modulation bandwidth of conventional separate confinement heterostructure (SCH) QD lasers was found to be limited to 5–8GHz at room temperature (Kamath *et al.*, 1997; Krebs *et al.*, 2001). The inhomogeneous linewidth broadening associated with nanostructure size dispersion is ultimately limited by growth technology, and it causes both the optical gain and differential gain to be reduced in the QD active region. Advancements in growth techniques using metalorganic chemical vapor deposition (MOCVD) reported high-quality InGaAs dots grown on a GaAs substrate operating at 1.28μm with improved gain and differential gain that yielded a modulation bandwidths as high as 12GHz (Kim *et al.*, 2004). Despite the slight improvement found in the modulation performance of such devices, the modulation bandwidth at higher current injection is still limited by the significant gain saturation typical of a QD active region (as shown in Fig. 10.20). The hot carrier effect in QDs is attributed to the increased carrier population at the higher energy dot states and also in the material surrounding the dots. With increasing carrier density, this is due primarily to the presence of a large number of available states in the two-dimensional electron-gas layer (wetting layer) compared to the dot itself.

As illustrated in Fig. 10.21, modulation bandwidths up to 30GHz were reported in InGaAs/GaAs SCH QD lasers by reducing the device's operating temperature as low as 80K (Bhattacharya *et al.*, 2000). Also shown in Fig. 10.21 are the differential gain and the *K*-factor as a function of temperature extracted from the response data measured at various
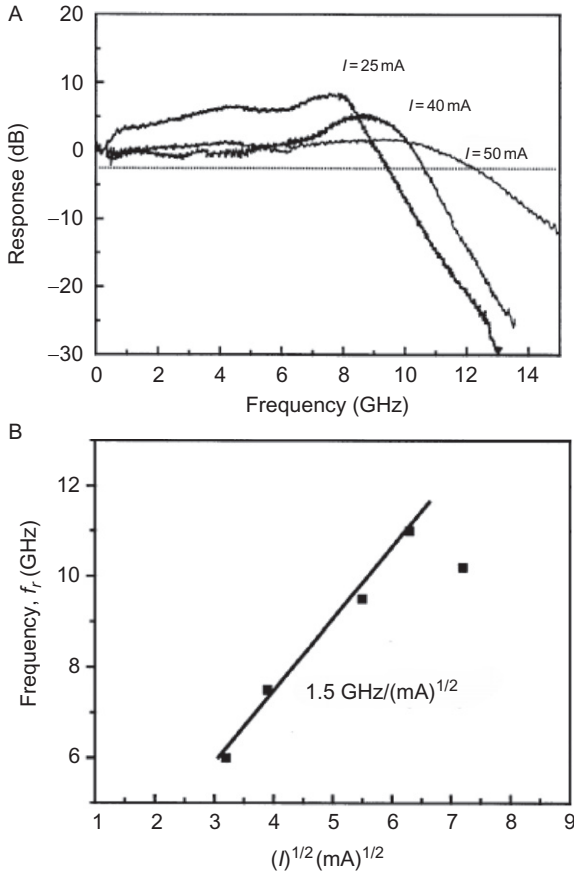
**FIGURE 10.20** (A) Room-temperature modulation response of the InGaAs/GaAs QD laser for various bias currents. (B) Relaxation oscillation frequency, $f_r$ as a function of the square root of bias current indicating the saturation of $f_r$ with bias current as a result of strong gain saturation in QD active region (Kim *et al.*, 2004).

temperatures. A larger differential gain at temperatures below $100\,\text{K}$ corresponds to reduced homogeneous broadening of the QD gain, while the *K*-factor reduction observed at lower temperature can be attributed to a reduced population of thermally generated holes, which then slows down the carrier-relaxation time. While the hot carrier effects in QDs have been studied for almost a decade now, several other methods were proposed to solve this problem; by p-doping the QDs or by using a tunnel-injection structure (Bhattacharya *et al.*, 2003; Deppe *et al.*, 2002). The following is a summary of the two techniques and their impacts on the modulation performance of the QD laser.
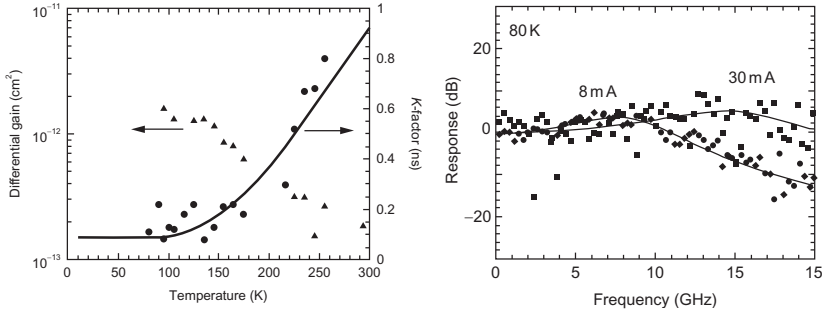
**FIGURE 10.21**    Left: Differential gain and *K*-factor as a function of temperature; right: modulation responses of a 200-μm-long In$_{0.4}$Ga$_{0.6}$As/GaAs QD laser measured at 80K. Responses measured for bias currents of 8 and 30mA indicating 3-dB bandwidths of ~10.5 and >20GHz, respectively (Bhattacharya *et al.*, 2000).

## 5.1. Effects of p-doping on the modulation performance of QD lasers

One of the major problems associated with the performance of QD lasers is the thermal broadening of carriers, especially holes due to their heavier effective mass and consequent tightly spaced energy levels. Thermal broadening of the dot hole population can significantly promote nonradiative recombination in the active region thereby suppressing the gain performance of QD lasers. One alternative solution to this problem is to introduce an excess acceptor (p-type) concentration into the QD barrier states either through direct or modulation acceptor doping.

As schematically illustrated in Fig. 10.22, the excess hole concentration from the p-doped barrier states is fed into the QD ground state to balance
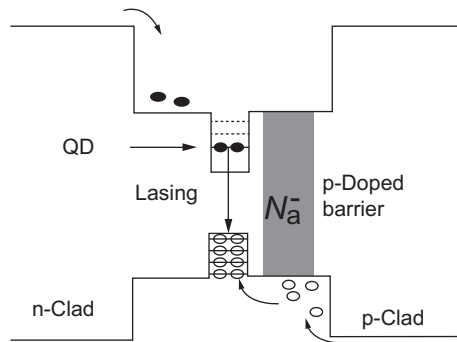


**FIGURE 10.22**    Increasing the QD ground-state hole population through modulation p-doping (Fathpour *et al.*, 2005a).

the effect of the thermally broadened hole distribution. While the concept of p-type doping of SL materials was initially introduced to improve the performance of QW lasers (Vahala and Zah, 1988; Zah et al., 1990), its impact on QD laser performance was expected to be even more significant due to the much lower electronic density of states (Yeh et al., 2000). Pioneering theoretical predictions and experimental observations have suggested that p-type doping of QD lasers should permit higher modal gain, higher differential gain, and reduced inhomogeneous linewidth broadening. Consequently, these improved characteristics were anticipated to improve overall modulation performance compared to conventional SCH laser diodes (Alexander et al., 2007; Deppe et al., 2002; Sandall et al., 2006; Shchekin et al., 2002). In spite of all the advantages, in side-by-side comparisons with undoped dots, p-doping of QD lasers has proven to only have a minor impact on the high-speed performance of the QD lasers with speeds limited to 10 Gb/s (Otsubo et al., 2004). This limitation is mainly attributed to the fact that the hole population is not thermally isolated from the higher dimensional states surrounding the dots. Recent studies on the modulation performance of QD lasers comparing p-type doped and undoped devices revealed that increasing the acceptor concentration in the material system can significantly increase the gain compression through increased internal losses in the active region and thereby hindering the maximum achievable bandwidth (Martinez et al., 2007). Other limiting factors associated with p-doped QD lasers include the reduced modal gain due to the inter-valance band absorption and increased nonradiative Auger recombination (Huberman et al., 1991; Marko et al., 2005a,b). Using p-doping, GaAs-based substrate QD lasers operating at 1.1 and 1.3 μm have achieved a maximum 3-dB bandwidth of 11 and 8 GHz, respectively, which are only slightly higher than those of the undoped devices (Fathpour et al., 2005b).

## 5.2. Modulation bandwidth enhancement using tunnel-injection QD laser structure

As mentioned in Section 5.1, hot carrier effects in SLs lead to a significant gain compression at room temperature which consequently limits the speed of the device under direct current modulation. One other method to reduce the hot carrier effect in lasers is through use of a tunnel-injection scheme. Tunnel-injection structures were first introduced to improve the performance of QW-based devices; achieving enhanced modulation bandwidths, higher characteristics temperatures, reduced Auger recombination, and reduced chirp. The reduction of hot carrier effects in these lasers is credited as the source of these improvements (Bhattacharya et al., 1996; Yoon et al., 1994; Zhang et al., 1997). It has been almost a decade since a similar concept was adopted for QDs and improvements in

tunnel-injection QD laser characteristics have been both theoretically and experimentally demonstrated (Asryan and Luryi, 2001; Bhattacharya *et al.*, 2003; Walter *et al.*, 2001). Most notably, it was found that tunnel-injection structures can significantly improve the dynamic properties of QD lasers (Ghosh *et al.*, 2002). To better understand the tunnel-injection structure and its associated carrier dynamics, the conduction band of a tunnel-injection QD laser is schematically shown in Fig. 10.23. In this structure, ''hot'' carriers are captured by the injector well and directly injected into the QD ground state via phonon-assisted tunneling, where typical tunneling rates are assumed to be fast enough ($\sim$1–2ps) to be immediately consumed by stimulated emission. As a result, hot carrier effects associated with barrier/wetting layers energy states as well as leakage currents can be significantly minimized. Since the majority of carriers are being initially described by a quasi-fermi distribution, then filtered by the phonon-assist process and injected near the ground-state energy level, the inhomogeneous linewidth broadening and associated gain compression are shown to reduce in tunnel-injection QD lasers (Ghosh *et al.*, 2002). This unique property is particularly beneficial for improving the speed of directly modulated devices including QD lasers. Over the past decade, use of tunnel-injection structures combined with the benefits of p-doping in QD lasers has proved to be very successful in developing faster devices, with demonstrations of improved modulation bandwidths and reduced frequency chirp. Using a tunnel-injection structure, a 3-dB bandwidth of 11 GHz with near-zero $\alpha$-factor is reported in a 1.3-$\mu$m QD laser operating at room temperature (Mi *et al.*, 2005). Recently, both p-doping and tunnel injection have been combined to achieve room-temperature 3-dB bandwidths of 25 and 13.5GHz in QD lasers operating
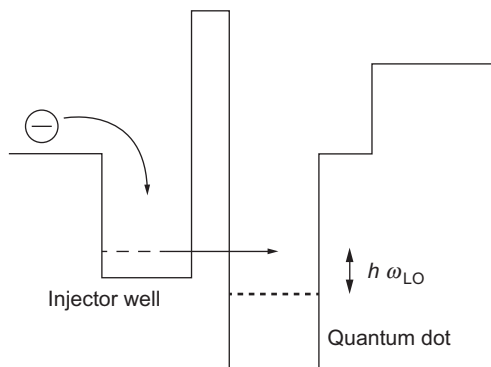


**FIGURE 10.23**   Conduction band diagram of a tunnel-injection QD laser structure (Bhattacharya *et al.*, 2003).

at 1.1 µm and excited state lasing at 1.22 µm, respectively (Fathpour *et al.*, 2005a; Lee *et al.*, 2011).

Although p-doping and tunnel injection were successfully shown to improve the modulation performance of QD lasers, combining the two methods in a single design still relies on complicated growth techniques which make it particularly difficult to achieve high-modulation bandwidths at the commercial communication wavelength of 1.3 µm. In addition to p-doping and tunnel injection, the dynamic properties of QD lasers also make their modulation characteristics under optical injection an interesting research area. The following section will discuss the impact of optical injection locking on the high-speed performance of directly modulated QD lasers.

## 5.3. Bandwidth enhancement in QD lasers using optical injection locking

Another method that can be called upon to improve the modulation characteristics of SLs is the optical injection-locking technique (Lang, 1982; Liu *et al.*, 1997; Mogensen *et al.*, 1985; Simpson and Liu, 1997). The mechanisms that induce significant improvement in the high-speed characteristics of injection-locked lasers have been extensively studied both theoretically and experimentally (Chrostowski *et al.*, 2007; Jin and Chuang, 2006; Lau *et al.*, 2009; Murakami *et al.*, 2003). In injection-locked laser systems, the key bandwidth improvement mechanism arises from the enhancement of the overall resonance frequency of the locked system. It has been shown that the enhancement of the resonance peak can exceed the limit set by the $K$-factor associated with the free-running laser parameters (Liu *et al.*, 1997; Simpson and Liu, 1997). Under constant injection strength, the injection-locked resonance peak is also strongly dependent on the frequency detuning between the master and slave lasers, as the poles in the overall injection-locked response are each a function of the detuning frequency. The highest degree of resonance frequency enhancement occurs at the positive frequency-detuning edge; however, this enhancement is accompanied by an undesired preresonance dip in the modulation response, limiting its suitability to narrow-band applications only (Lau *et al.*, 2009).

A recent investigation on modulation characteristics of an injection-locked quantum-dash (QDash) FP laser system showed that the undesired preresonance dip can be virtually eliminated by manipulating the device-operating parameters such as the free-running relaxation oscillation frequency, free-running damping rate, and especially the slave $\alpha$-factor since it was found to be highly variable with optical power (Naderi *et al.*, 2009). In the case of QD nanostructure lasers, a 3-dB bandwidth of 16.3 GHz was reported by Terry *et al.* in an injection-locked

QD DFB laser; the improvement was reported to be $4\times$ its free-running value (Terry *et al.*, 2008).

Here the high-speed modulation characteristics of an injection-locked FP QD laser under ultra-strong injection are presented with a focus on the enhancement of the modulation bandwidth. The coupled system consists of a directly modulated QD slave injection locked by a DFB laser as the master. Experimental observations indicate that under strong injection strengths and particular frequency-detuning values, the injection-locked QD laser has a unique modulation response that differs from the typical modulation response observed in injection-locked systems. This unique response is characterized by a rapid low-frequency rise along with a slow high-frequency roll-off that enhances the 3-dB bandwidth of the injection-locked system at the expense of losing modulation efficiency of about 22 dB at frequencies below 1 GHz. There are two benefits in having this unique response. One benefit is that the resonance frequency enhancement does not experience the preresonance dip that usually limits the amount of useful bandwidth for the high-speed injection-locked response (Lau *et al.*, 2009). The second benefit is the improvement in the high-frequency roll-off that extends the bandwidth. Also, a 3-dB bandwidth improvement of greater than eight times compared to the free-running slave laser is observed. The layer structure of the QD slave laser under investigation is illustrated in Fig. 10.24A. The QD slave laser was grown on an $n^+$-GaAs substrate using molecular-beam epitaxy. The DWELL active region consists of six layers of InAs QDs embedded in compressively strained $In_{0.15}Ga_{0.85}As$ QWs each separated by 30-nm undoped GaAs barrier layers. Three micrometers-wide ridge waveguides laser bars were fabricated using standard processing techniques and cleaved into 300-µm-long cavity lengths with front and back facets HR/HR coated at 80% and 95%, respectively, to increase the ground-state gain. The light–
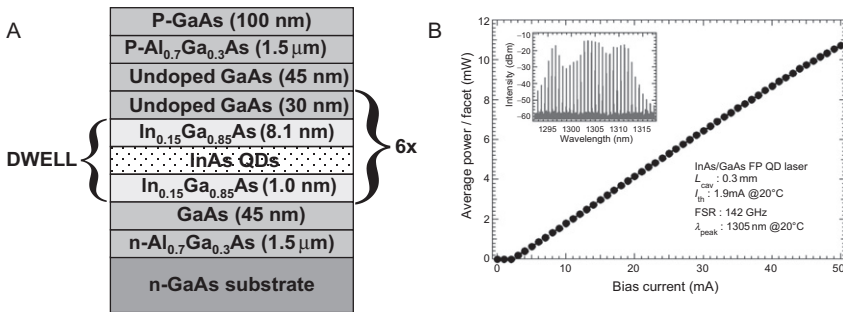


**FIGURE 10.24**  (A) Epitaxial layer structure of the InAs/GaAs QD slave laser, (B) light–current characteristics and emission spectra of the QD slave laser under investigation.
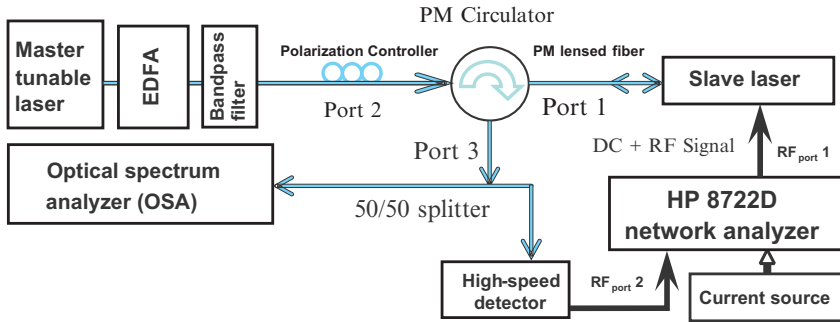
**FIGURE 10.25**    Block diagram of the injection-locking experimental setup.

current characteristics and the emission spectra of the slave laser under investigation are shown in Fig. 10.24B. The QD laser was found to have a threshold current density of $211\,A/cm^2$ (1.9 mA) with a slope efficiency of 0.23 W/A, and a nominal emission wavelength of approximately 1305 nm at room temperature.

A schematic of the experimental setup used to measure the high-speed characteristics of the injection-locked QD laser is shown in Fig. 10.25. The master laser was a Fujitsu temperature-tunable QW DFB laser with a nominal emission wavelength of 1315 nm. The master laser's output was fiber pigtailed into a single-mode polarization-maintained (PM) fiber that was coupled into the second port of a three-port PM circulator. The PM circulator is designed to operate around 1310 nm and has an isolation level of >20 dB. The biased slave laser was kept at 20°C. For all cases, the slave laser bias current was kept constant at 5 mA and emits a total output power of 0.79 mW. The pump current on the DFB master laser was adjusted to obtain an external power ratio of 15 dB, which corresponds to 24.4 mW available injected power at the slave facet.

Figure 10.26 represents the normalized modulation responses for the free-running laser along with zero, positive, and negative detuning injection-locked responses for an ultra-strong external power ratio of 15 dB. The positive frequency-detuning cases (top graph) indicate a bandwidth enhancement of 8.1 times, and the negative frequency-detuning cases (bottom graph) indicate a 3-dB bandwidth enhancement of 4.7 times compared to the free-running case. It is important to note that on the positive detuning side, the maximum bandwidth occurs at detuning cases that have a unique shape in the modulation response that are not seen for the QDash laser (Naderi *et al.*, 2009). This novel shape, which has a fast low-frequency rise and a slow high-frequency roll-off, is characteristic of situations that have a small zero, Z, in the numerator of the modulation response function (Naderi *et al.*, 2009). This small Z is enabled by the
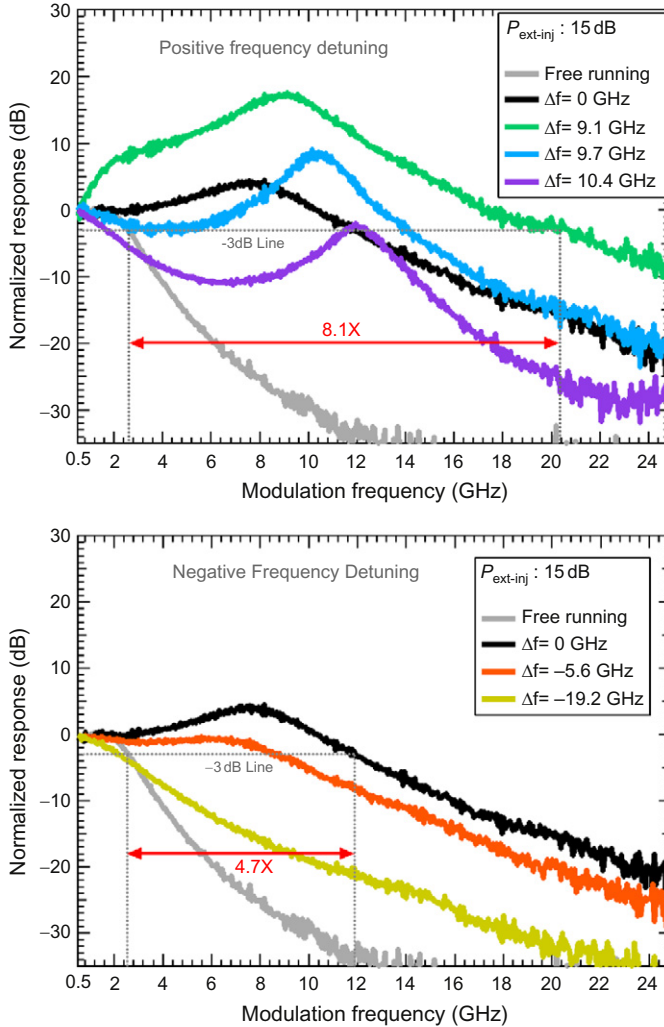
**FIGURE 10.26** Normalized modulation responses under positive (top) and negative (bottom) frequency-detuning conditions for $P_{ext-inj}$=15dB, indicating 8.1× and 4.7× improvement in 3-dB bandwidth, respectively, compared to the free-running case.

relatively small $\alpha$-factor in the QD laser. Further positive frequency-detuning cases suffer from the undesired preresonance dip between the DC value and the enhanced resonance. The unique broadband responses along with their associated small $\alpha_H$-factor values show that injection-locked QD FP lasers can be optimized as an integrated high-speed photonic transmitter for future high-speed links.

## 6. CONCLUSION AND OUTLOOK

Since the inception of the QD laser, many important results have been achieved, pushing the frontiers of SLs and the range of applications where they excel into a new era. The driving force behind these achievements is the unique properties of the QD media. In particular, the area of GaAs-based QD lasers has been the focus of intense research efforts for almost two decades now. We have reviewed the advances for such lasers emitting at wavelengths longer than 1.2 μm, concentrating on four key areas, namely, the record-low-threshold currents as well as the impressive temperature stability these lasers possess, the extreme range of linewidth enhancement factors possible in these devices, the ultralow linewidth–power product and insensitivity to optical feedback of QD DFB lasers and finally, the progress achieved to date in achieving higher modulation bandwidths in directly modulated and injection-locked QD lasers.

One of the immediate achievements for GaAs-based QD lasers was the demonstration of extremely low-threshold currents. Broadly speaking, there were two key technology advancements which enabled the realization of sub-20 A/cm$^2$ threshold currents. These were the introduction of DWELL design and the development of high growth temperature spacer layers for multi-stack QD lasers. Several groups have now routinely reported threshold current densities in the vicinity of 10 A/cm$^2$ per dot stack.

The quest for a temperature-immune SL based on full three-dimensional carrier confinement, initially proposed by Arakawa in 1982, has eluded the QD laser community from the offset. Although, in practice, several intrinsic properties limit the realization of such a laser, nevertheless, the QD laser has made substantive progress. The initially reported sensitivity of the threshold current to temperature was poor; no better than QW lasers emitting at similar wavelengths. However, great strides have been made in recent years to improve their initially modest temperature stability. p-Type modulation doping, tunnel-injection techniques, and shape engineering of the dots were central in improving the overall temperature stability of QD lasers, ultimately enabling temperature operation beyond 200 °C. The application of high-reflectivity facet coatings at the same time ensured respectable output powers. GaAs-based QD lasers with output powers of 1 mW operating to 220 °C have now been reported. Applications in hot environments such as what would be required in oil and gas sensing are now gaining attention, not to mention the attractiveness of uncooled emitters.

A myriad of techniques have been called upon to measure the linewidth enhancement factor, elucidating the extreme nature of the amplitude-phase coupling in QD lasers, relative to conventional SLs. Values ranging from negative 20 to positive values approaching 60 have

been reported, demonstrating the wide range of values this crucial device parameter can take. Much work has been undertaken to model and understand its behavior and how it can be manipulated. Dispersion management of optical pulses in fiber-optic systems is an area of interest where this can be exploited.

A combination of a lower linewidth enhancement factor combined with a smaller population inversion factor has resulted in the demonstration of more than an order of magnitude narrower linewidth for QD DFBs compared to commercial QW DFBs. Linewidths on the order of hundreds of kilohertz have been reported at milliwatt optical power levels. Another demonstration of the superiority of QD DFBs is their exceptional resistance to optical feedback. This property positions the QD DFB as an ideal emitter to operate in isolator-free fiber-optic communication networks.

The closing section of this chapter focussed on the progress to date in achieving higher modulation bandwidths in directly modulated and injection-locked QD lasers. This is the one area where the initial prediction of the expected superiority of QD lasers compared to QW lasers has been difficult to demonstrate. Room-temperature modulation bandwidths were found to be limited to about 12 GHz. Several inherent factors were touted as being responsible and included the slow carrier-relaxation time, inhomogeneous broadening and hot carrier effects. Interestingly, by dramatically reducing the operating temperature to as low as 80 K, modulation bandwidths as high as 30 GHz were observed. Techniques to mimic a lower temperature carrier distribution were initiated by use of tunnel-injection schemes; however, the best modulation bandwidths achieved were associated with excited state emission rather than from the ground state. In all, optical injection techniques have been the most successful in enhancing the 3-dB at which QD lasers can be modulated. Current values at room temperature for QD ground-state emission stand at 20 GHz.

As such, GaAs-based QD lasers have proven their large potential for future high-speed optical communication applications as well as new ventures such as those required in high-temperature applications. This progress is expected to continue as a fresh program of studies is undertaken to optimize and develop these lasers beyond their current standing. Thus going forward, QD lasers are expected to remain at the forefront of modern photonics.

## REFERENCES

Agrawal, G. P. (1990). *IEEE J. Quantum Electron.* **26,** 1901–1909.

Agrawal, G. P. (2002). *Fiber-Optic Communication Systems.* Wiley Interscience, New York, pp. 478–512.

Agrawal, G. P., Duan, G. H., and Gallion, P. (1992). *Electron Lett.* **28,** 1773–1774.

Alexander, R. R., Childs, D., Agarwal, H., Groom, K. M., Liu, H. Y., Hopkinson, M., Hogg, R. A., Ishida, M., Yamamoto, T., Sugawara, M., *et al.* (2007). *IEEE J. Quantum Electron.* **43**(12), 1129–1139.

Arakawa, Y., and Sakaki, H. (1982). *Appl. Phys. Lett.* **40,** 939–941.

Asada, M., Miyamoto, Y., and Suematsu, Y. (1986). *IEEE J. Quantum Electron.* **22**(9), 1915–1921.

Asryan, L., and Luryi, S. (2001). *IEEE J. Quantum Electron.* **37**(7), 905–910.

Asryan, L. V., and Suris, R. A. (1997). *Electron. Lett.* **33,** 1871–1872.

Azouigui, S., Cong, D.-Y., Martinez, A., Merghem, K., Zou, Q., Provost, J.-G., Dagens, B., Fischer, M., Gershuetz, F., Koeth, J., *et al.* (2011). *IEEE Photon. Technol. Lett.* **23**(9), 582–584.

Bayer, M., and Forchel, A. (2002). *Phys. Rev. B* **65**(4), 41308-1–41308-4.

Belenky, G. L., Reynolds, C. L., Donetsky, D. V., Jr., Shtengel, G. E., Hybertsen, M. S., Alam, M. A., Baraff, G. A., Smith, R. K., Kazarinov, R. F., Winn, J., *et al.* (1999). *IEEE J. Quantum Electron.* **35,** 1515–1520.

Berg, T. W., and Mork, J. (2003). *Appl. Phys. Lett.* **82,** 3083–3085.

Bhattacharya, P., Ghosh, S., Pradhan, S., Singh, J., Zong-Kwei, W., Urayama, J., Kyoungsik, K., and Norris, T. B. (2003). *IEEE J. Quantum Electron.* **39**(8), 952–962.

Bhattacharya, P., Klotzkin, D., Qasaimeh, O., Zhou, W. D., Krishna, S., and Zhu, D. H. (2000). *IEEE J. Sel. Top. Quantum Electron.* **6**(3), 426–438.

Bhattacharya, P., Singh, J., Yoon, H., Zhang, X., Gutierrez-Aitken, A., and Lam, Y. (1996). *IEEE J. Quantum Electron.* **32**(9), 1620–1629.

Bimberg, D., Kirstaedter, N., Ledentsov, N. N., Alferov, Zh.I., Kop'ev, P. S., and Ustinov, V. M. (1997). *IEEE J. Sel. Top. Quantum Electron.* **3,** 196–205.

Chand, N., Becker, E. E., Van Der Zeil, J. P., Chu, S. N. G., and Dutta, N. K. (1991). *Appl. Phys. Lett.* **58,** 1704–1706.

Chrostowski, L., Faraji, B., Hofmann, W., Amann, M. C., Wieczorek, S., and Chow, W. W. (2007). *IEEE J. Sel. Top. Quantum Electron.* **13**(5), 1200–1208.

Coldren, L. A., and Corzine, S. W. (1995). Diode Lasers and Photonics Integrated Circuits. John Wiley & Sons, New York.

Crowley, M. T., Marko, I. P., Massé, N. F., Andreev, A. D., Tomić, S., Sweeney, S. J., O'Reilly, E. P., and Adams, A. R. (2009). *IEEE J. Sel. Top. Quantum Electron.* **15,** 799–807.

Dagens, B., Markus, A., Chen, J. X., Provost, J. G., Make, D., Le Gouezigou, O., Landreau, J., Fiore, A., and Thedrez, B. (2005). *Electron. Lett.* **41,** 323–324.

Deppe, D. G., Huang, H., and Shchekin, O. B. (2002). *IEEE J. Quantum Electron.* **38**(12), 1587–1593.

Deppe, D. G., Shavritranuruk, K., Ozgur, G., Chen, H., and Freisem, S. (2009). *Electron. Lett.* **45,** 54.

Devaux, F., Sorel, Y., and Kerdiles, J. F. (1993). *J. Lightw. Technol.* **11,** 1937–1940.

Eliseev, P. G., Li, H., Stintz, A., Liu, G. T., Newell, T. C., Malloy, K. J., and Lester, L. F. (2000). *Appl. Phys. Lett.* **77,** 262.

Fathpour, S., Mi, Z., and Bhattacharya, P. (2005a). *J. Phys. D Appl. Phys.* **38**(13), 2103–2111.

Fathpour, S., Mi, Z., and Bhattacharya, P. (2005b). *IEEE Photon. Technol. Lett.* **17**(11), 2250–2252.

Fathpour, S., Mi, Z., Bhattacharya, P., Kovsh, A. R., Mikhrin, S. S., Krestnikov, I. L., Kozhukhov, A. V., and Ledentsov, N. N. (2004). *Appl. Phys. Lett.* **85,** 5164.

Fleming, M. W., and Mooradian, A. (1981). *IEEE J. Quantum Electron.* **17,** 44–59.

Ghosh, S., Pradhan, S., and Bhattacharya, P. (2002). *Appl. Phys. Lett.* **81**(16), 3055–3057.

Girardin, F., Duan, G. H., and Gallion, P. (1996). *IEEE Photon. Technol. Lett.* **8,** 334–336.

Giuliani, G., Donati, S., Villafranca, A., Lasobras, J., Garces, I., Chacinski, M., Schatz, R., Kouloumentas, C., Klonidis, D., Tomkos, I., *et al.* (2007). Round-Robin Measurements of Linewidth Enhancement Factor of Semiconductor Lasers in COST 288 Action, CB9-2-WED. CLEO Europe/IQEC.

Goobar, E., Gillner, L., Schatz, R., Broberg, B., Nilsson, S., and Tanbunek, T. (1988). *Electron. Lett.* **24,** 746–747.

Goulding, D., Hegarty, S. P., and Huyet, G. (2007). *IEEE J. Sel. Top. Quantum Electron.* **13,** 1257–1260.

Grillot, F., Dagens, B., Provost, J. G., Su, H., and Lester, L. F. (2008). *IEEE J. Quantum Electron.* **44,** 946–951.

Grillot, F., Naderi, N. A., Pochet, M., Lin, C.-Y., and Lester, L. F. (2008). *Appl. Phys. Lett.* **93,** 191108.

Grillot, F., Thredrez, B., Py, J., Gauther-Lafaye, O., Voiriot, V., and Lafragette, J. L. (2002). *IEEE Photon. Technol. Lett.* **14**(1), 101–103.

Hakki, B. W., and Paoli, T. L. (1975). *J. Appl. Phys.* **46,** 1299–1306.

Harder, C., Vahala, K., and Yariv, A. (1983). *Appl. Phys. Lett.* **42,** 328–330.

Hegarty, S. P., Corbett, B., McInerney, J. G., and Huyet, G. (2005). *Electron. Lett.* **41,** 416–418.

Henning, I. D., and Collins, J. V. (1983). *Electron. Lett.* **19,** 927–929.

Henry, C. H. (1982). *IEEE J. Quantum Electron.* **18,** 259–264.

Higashi, T., Sweeney, S. J., Phillips, A. F., Adams, A. R., O'Reilly, E. P., Uchida, T., and Fujii, T. (1999). *IEEE J. Sel. Top. Quantum Electron.* **5,** 413–419.

Huberman, M. L., Ksendzov, A., Larsson, A., Terhune, R., and Maserjian, J. (1991). *Phys. Rev. B* **44**(3), 1128–1133.

Hui, R., Mecozzi, A., D'Ottavi, A., and Spano, P. (1990). *Electron. Lett.* **26,** 997–998.

Ishida, M., Hatori, N., Otsubo, K., Yamamoto, T., Nakata, Y., Ebe, H., Sugawara, M., and Arakawa, Y. (2007). *Electron. Lett.* **43**(4), 219–222.

Jin, X., and Chuang, S. L. (2006). *Solid State Electron.* **50**(6), 1141–1149.

Kamath, K. K., Phillips, J., Jiang, H., Singh, J., and Bhattacharya, P. (1997). *Appl. Phys. Lett.* **70** (22), 2952–2953.

Kim, J., Su, H., Minin, S., and Chuang, S.-L. (2006a). *IEEE Photon. Technol. Lett.* **18**(9), 1022–1024.

Kim, J., Su, H., Minin, S., and Chuang, S.-L. (2006b). *IEEE J Quantum Electron.* **42**(9), 942–952.

Kim, S. M., Wang, Y., Keever, M., and Harris, J. S. (2004). *IEEE Photon. Technol. Lett.* **16**(2), 377–379.

Kirstaedter, N., Ledenstov, N. N., Grundmann, M., Bimberg, D., Ustinov, V. M., Ruvimov, S. S., Maximov, M. V., Kop'ev, P. S., Alferov, Z., Richter, U., *et al.* (1994). *Electron. Lett.* **30,** 1416–1417.

Klotzkin, D., Kamath, K., Vineberg, K., Bhattacharya, P., Murty, R., and Laskar, J. (1998). *IEEE Photon. Technol. Lett.* **10**(7), 932–934.

Krebs, R., Klopf, F., Rennon, S., Reithmaier, J. P., and Forchel, A. (2001). *Electron. Lett.* **37**(20), 1223–1225.

Kruger, U., and Kruger, K. (1995). *J. Lightw. Technol.* **13,** 592–597.

Lang, R. (1982). *IEEE J. Quantum Electron.* **18**(6), 976–983.

Lau, E. K., Wong, L. J., and Wu, M. C. (2009). *IEEE J. Sel. Top. Quantum Electron.* **15**(3), 618–633.

Lau, K. Y., and Yariv, A. (1985). *IEEE J. Quantum Electron.* **21**(2), 121–138.

Ledentsov, N. N., Shchukin, V. A., Grundmann, M., Kirstaedter, N., Bohrer, J., Schmidt, O., Bimberg, D., Ustinov, V. M., Egorov, A. Y., Zhukov, A. E., *et al.* (1996). *Phys. Rev. B* **54,** 8743–8750.

Lee, C.-S., Bhattacharya, P., Frost, T., and Guo, W. (2011). *Appl. Phys. Lett.* **98**(1), 011103-1–011103-3.

Lester, L. F., Stintz, A., Li, H., Newell, T. C., Pease, E. A., Fuchs, B. A., and Malloy, K. J. (1999). *IEEE Photon. Technol. Lett.* **11,** 931–933.

Liu, J. M., Chen, H. F., Meng, X. J., and Simpson, T. B. (1997). *IEEE Photon. Technol. Lett.* **9**(10), 1325–1327.

Liu, G., Jin, X., and Chuang, S. L. (2001). *IEEE Photon. Technol. Lett.* **13,** 430–432.

Liu, H. Y., Sellers, I. R., Badcock, T. J., Mowbray, D. J., Skolnick, M. S., Groom, K. M., Gutierrez, M., Hopkinson, M., Ng, J. S., and David, J. P. R. (2004). *Appl. Phys. Lett.* **85,** 704–706.

Liu, G. T., Stintz, A., Li, H., Malloy, K. J., and Lester, L. F. (1999). *Electron. Lett.* **35,** 1163–1165.

Liu, G. T., Stintz, A., Li, H., Newell, T. C., Gray, A. L., Varangis, P. M., Malloy, K. J., and Lester, L. F. (2000). *IEEE J. Quantum Electron.* **36,** 1272–1279.

Mao, M.-H., Heinrichsdorff, F., Krost, A., and Bimberg, D. (1997). *Electron. Lett.* **33**(19), 1641–1642.

Marciante, J., and Agrawal, G. P. (1996). *IEEE J. Quantum Electron.* **32,** 590–596.

Marko, I. P., Adams, A. R., Sweeney, S. J., Sellers, I. R., Mowbray, D. J., Skolnick, M. S., Liu, H. Y., and Groom, K. M. (2005). *IEEE J. Sel. Top. Quantum Electron.* **11,** 1041–1047.

Marko, I. P., Masse, N. F., Sweeney, S. J., Andreev, A. D., Adams, A. R., Hatori, N., and Sugawara, M. (2005). *Appl. Phys. Lett.* **87,** 211114-1–211114-3.

Martinez, A., Li, Y., and Lester, L. F. (2007). *Appl. Phys. Lett.* **90**(25), 251101-1–251101-3.

Matthews, M. R., Cameron, K. H., Wyatt, R., and Devlin, W. J. (1985). *Electron. Lett.* **21,** 113–115.

Matthews, D. R., Summers, H. D., and Smowton, P. M. (2002). *Appl. Phys. Lett.* **81**(26), 4904–4906.

Melnik, S., and Huyet, G. (2006). *Opt. Expr.* **14,** 2950–2955.

Mi, Z., Bhattacharya, P., and Fathpour, S. (2005). *Appl. Phys. Lett.* **86**(15), 153109-1–153109-3.

Mogensen, F., Olesen, H., and Jacobsen, G. (1985). *IEEE J. Quantum Electron.* **21**(7), 784–793.

Mukai, K., Ohtsuka, N., Sugawara, M., and Yamazaki, S. (1994). *Jap. J. Appl. Phys.* **33**(12A), 1710–1712.

Murakami, A., Kawashima, K., and Atsuki, K. (2003). *IEEE J. Quantum Electron.* **39**(10), 1196–1204.

Naderi, N. A., Pochet, M., Grillot, F., Terry, N. B., Kovanis, V., and Lester, L. F. (2009). *IEEE J. Sel. Top. Quantum Electron.* **15**(3), 563–571.

Nakahara, K., Tsuchiya, T., Kitatani, T., Shinoda, K., Taniguchi, T., Kikawa, T., Aoki, M., and Mukaikubo, M. (2007). *IEEE Photon. Technol. Lett.* **19**(19), 1436–1438.

Newell, T. C., Bossert, D. J., Stintz, A., Fuchs, B., Malloy, K. J., and Lester, L. F. (1999). *IEEE Photon. Technol. Lett.* **11,** 1527–1529.

Okai, M. (1994). *J. Appl. Phys.* **75,** 1–29.

Okai, M., Suzuki, M., Taniwatari, T., and Chinone, N. (1994). *Jpn. J. Appl. Phys.* **33,** 2563–2570.

Okoshi, T., Kikuchi, K., and Nakayama, A. (1980). *Electron. Lett.* **16,** 630–631.

Olesen, H., Tromborg, B., Lassen, H. E., and Pan, X. (1992). *Electron. Lett.* **28,** 444–446.

Olshansky, R., Hill, P., Lanzisera, V., and Powazinik, W. (1987). *IEEE J. Quantum Electron.* **23**(9), 1410–1418.

Osinski, M., and Buus, J. (1987). *IEEE J. Quantum Electron.* **23,** 9–29.

Otsubo, K., Hatori, N., Ishida, M., Okumura, S., Akiyama, T., Nakata, Y., Ebe, H., Sugawara, M., and Arakawa, Y. (2004). *Jpn. J. Appl. Phys.* **43**(8B), 1124–1126.

Palavicini, C., Campuzano, G., Thedrez, B., Jaouen, Y., and Gallion, P. (2003). *IEEE Photon. Technol. Lett.* **15,** 1683–1685.

Pan, X., Tromborg, B., and Olesen, H. (1991). *IEEE Photon. Technol. Lett.* **3,** 112–114.

Patzak, E., Sugimura, A. S., Saito, S., Mukai, T., and Olesen, H. (1983). *Electron. Lett.* **19,** 1026–1027.

Petermann, K. (1991). Laser Diode Modulation and Noise. Kluwer Academic Publisher, Dordrecht.

Provost, J. G., and Grillot, F. (2011). *IEEE Photon. J.* **3,** 476–488.

QD Laser Inc (2011). *Laser Focus World* **47**(7), 9.

Qiu, Y., Gogna, P., Forouhar, S., Stintz, A., and Lester, L. F. (2001). *Appl. Phys. Lett.* **79,** 3570–3572.

Rossetti, M., Fiore, A., Sęk, G., Zinoni, C., and Li, L. (2009). *J. Appl. Phys.* **106,** 023105-1–023105-8.

Royset, A., Bjerkan, L., Myhre, D., and Hafskjaer, L. (1994). *Electron. Lett.* **30,** 710–712.

Salhi, A., Rainó, G., Fortunato, L., Tasco, V., Visimberga, G., Martiradonna, L., Todaro, M. T., De Giorgi, M., Cingolani, R., Trampert, A., De Vittorio, M., and Passaseo, A. (2008). *J. Sel. Topics Quantum Electron.* **14,** 1188.

Sandall, I. C., Smowton, P. M., and Thomson, J. D. (2006). *Appl. Phys. Lett.* **89**(15), 151118-1–151118-3.

Saunders, R. A., King, J. P., and Hardcastle, I. (1994). *Electron. Lett.* **30,** 1336–1338.

Sellers, I. R., Liu, H. Y., Groom, K. M., Childs, D. T., Robbins, D., Badcock, T. J., Hopkinson, M., Mowbray, D. J., and Skolnick, M. S. (2004). *Electron. Lett.* **40,** 1412–1413.

Shchekin, O. B., Ahn, J., and Deppe, D. G. (2002). *Electron. Lett.* **38,** 712–713.

Shchekin, O. B., and Deppe, D. G. (2002). *Appl. Phys. Lett.* **80,** 3277–3279.

Shimizu, H., Saravanan, S., Yoshida, J., Ibe, S., and Yokouchi, N. (2005). *Jpn. J. Appl. Phys.* **44,** L1103.

Shimpe, R., Bowers, J. E., and Koch, T. L. (1986). *Electron. Lett.* **22,** 453–454.

Simpson, T. B., and Liu, J. M. (1997). *IEEE Photon. Technol. Lett.* **9**(10), 1322–1324.

Smowton, P. M., George, A., Sandall, I. C., Hopkinson, M., and Liu, H. Y. (2008). *IEEE J. Sel. Top. Quantum Electron.* **14,** 1162–1170.

Smowton, P. M., Pearce, E. J., Schneider, H. C., Chow, W. W., and Hopkinson, M. (2003). *Appl. Phys. Lett.* **81,** 3251–3253.

Sorin, W. V., Chang, K. W., Conrad, G. A., and Hernday, P. R. (1992). *J. Lightw. Technol.* **10,** 787–793.

Srinivasan, R. C., and Cartledge, J. C. (1995). *IEEE Photon. Technol. Lett.* **7,** 1327–1329.

Su, H., and Lester, L. F. (2005). *J. Phys. D Appl. Phys.* **38**(13), 2112–2118.

Su, H., Zhang, L., Gray, A. L., Wang, R., Newell, T. C., Malloy, K. J., and Lester, L. F. (2003). *IEEE Photon. Technol. Lett.* **15,** 1504–1506.

Su, H., Zhang, L., Gray, A. L., Wang, R., Newell, T. C., Malloy, K. J., and Lester, L. F. (2004). *IEEE Photon. Technol. Lett.* **16,** 2206–2208.

Su, H., Zhang, L., Gray, A. L., Wang, R., Varangis, P. M., and Lester, L. F. (2005). *Proc. SPIE* **5722,** 72–79.

Takano, S., Sasaki, T., Yamada, H., Kitamura, M., and Mito, I. (1989). *Electron. Lett.* **25,** 356–357.

Terry, N. B., Naderi, N. A., Pochet, M., Moscho, A. J., Lester, L. F., and Kovanis, V. (2008). *Electron. Lett* **44**(15), 904–905.

Toffano, Z., Destrez, A., Birocheau, C., and Hassine, L. (1992). *Electron. Lett.* **28,** 9–11.

Tokranov, V., Yakimov, M., Katsnelson, A., Lamberti, M., and Oktyabrsky, S. (2003). *Appl. Phys. Lett.* **83,** 833–835.

Ukhanov, A. A. (2004). PhD dissertation. University of New Mexico.

Urayama, J., Norris, T., Singh, J., and Bhattacharya, P. (2001). *Phys. Rev. Lett.* **86**(21), 4930–4933.

Uskov, A. V., O'Reilly, E. P., McPeake, D., Ledentsov, N. N., Bimberg, D., and Huyet, G. (2004). *Appl. Phys. Lett.* **84,** 272–274.

Vahala, K. J., and Zah, C. E. (1988). *Appl. Phys. Lett.* **52**(23), 1945–1947.

Villafranca, A., Lázaro, J. A., Salinas, I., and Garcés, I. (2005). *IEEE Photon. Technol. Lett.* **17,** 2268–2270.

Villafranca, A., Villafranca, A., Giuliani, G., and Garces, I. (2009). *IEEE Photon. Technol. Lett.* **21,** 1256–1258.

Vodhanel, R. S., and Tsuji, S. (1988). *Electron. Lett.* **24,** 1359–1361.

Walter, G., Holonyak, N., Jr., Ryou, J. H., and Dupuis, R. D. (2001). *Appl. Phys. Lett.* **79**(20), 3215–3217.

Weisser, S., Esquivias, I., Tasker, P. J., Ralston, J. D., and Rosenzweig, J. (1994). *Photon. Technol. Lett.* **6**(7), 1041–1135.

Wellford, D., and Alexander, S. B. (1985). *J. Lightw. Technol.* **3,** 1092–1099.

Wenzel, H., Wunsche, H. J., and Bandelow, U. (1991). *Electron. Lett.* **27,** 2301–2302.

Yeh, N.-T., Lee, J.-M., Nee, T.-E., and Chyi, J.-I. (2000). *IEEE Photon. Technol. Lett.* **12**(9), 1123–1125.

Yoon, H., Sun, H. C., and Bhattacharya, P. (1994). *Electron. Lett.* **30**(20), 1675–1677.

Yu, Y., Giuliani, G., and Donati, S. (2004). *IEEE Photon. Technol. Lett.* **16,** 990–992.

Zah, C. E., Bhat, R., Menocal, S. G., Favire, F., Andreadakis, N. C., Koza, M. A., Caneau, C., Schwarz, S. A., Lo, Y., and Lee, T. P. (1990). *IEEE Photon. Technol. Lett.* **2**(4), 231–233.

Zhang, X., Gutierrez-Aitken, A., Klotzkin, D., Bhattacharya, P., Caneau, C., and Bhat, R. (1997). *IEEE J. Sel. Top. Quantum Electron.* **3**(2), 309–314.

Zhang, L., Wang, R., Zou, Z., Gray, A., Olona, L., Newell, T., Webb, D., Varangis, P., and Lester, L. F. (2003). Optical Fiber Communication Conference, Technical Digest (Optical Society of America). paper FG2.

Zhang, T., Zhu, N. H., Zhang, B. H., and Zhang, X. (2007). *IEEE Photon. Technol. Lett.* **19,** 227–229.

Zhao, B., and Yariv, A. (1999). *In* ''Semiconductor Lasers I Fundamentals,'' (Eli Kapon, ed.), pp. 1–109. Academic Press.